

Nuclear Properties According to the Thomas-Fermi Model

W.D. Myers and W.J. Swiatecki

Nuclear Science Division
Lawrence Berkeley Laboratory
University of California
Berkeley, California 94720

January 1995

DISCLAIMER

This document was prepared as an account of work sponsored by the United States Government. While this document is believed to contain correct information, neither the United States Government nor any agency thereof, nor the Regents of the University of California, nor any of their employees, makes any warranty, express or implied, or assumes any legal responsibility for the accuracy, completeness, or usefulness of any information, apparatus, product, or process disclosed, or represents that its use would not infringe privately owned rights. Reference herein to any specific commercial product, process, or service by its trade name, trademark, manufacturer, or otherwise, does not necessarily constitute or imply its endorsement, recommendation, or favoring by the United States Government or any agency thereof, or the Regents of the University of California. The views and opinions of authors expressed herein do not necessarily state or reflect those of the United States Government or any agency thereof or the Regents of the University of California.

Abstract

In order to formulate a statistical model of nuclear properties we combine the Thomas-Fermi assumption of two fermions per h^3 of phase space with an effective interaction between nucleons that contains seven adjustable parameters. After allowing for shell effects, an even-odd correction and a congruence energy ("Wigner Term"), six of the seven parameters were fitted to 1654 ground state masses of nuclei with $N, Z \geq 8$, together with a constraint that ensures agreement with measured values of the nuclear surface diffuseness. The RMS deviation in the fit to masses was 0.655 MeV, and the calculated values exhibit no drastic discrepancies even for $A = 3$.

Calculated sizes of nuclear charge distributions agree closely with measurements. Calculated fission barriers were compared with 40 measured values down to ^{75}Br . For $Z \geq 88$ the agreement is almost perfect. For $Z < 88$ the trend of the measurements seems to confirm the expectation that the congruence energy should double its magnitude for strongly necked-in saddle-point shapes.

A seventh (density-dependence) parameter in the effective interaction can be adjusted to ensure fair agreement with the measured energy-dependence of the optical model potential in the range from -70 MeV to 180 MeV.

The model is used to predict properties of nuclear and neutron matter (including their compressibilities). A table of some 9000 calculated ground state masses of nuclei up to $Z = 135$ has been prepared.

1. Introduction

A degenerate gas of fermions in an external potential is characterized by a density of 2 particles per volume h^3 of phase space. In 1927 L.H. Thomas [1] and, independently, E. Fermi [2] made this simple observation the basis of a beautiful semi-classical, statistical theory of atomic properties [3]. The same method has been applied to the nuclear many-body problem, treated in the mean-field approximation.

In the atomic case the mean field is produced by well-defined electrostatic forces, and there are no adjustable parameters in the theory. In the nuclear case one needs to introduce effective nucleon-nucleon interactions that are not uniquely defined and which contain adjustable parameters. As a result there exist today dozens of nuclear Thomas-Fermi models characterized by different effective interactions (as well as by different refinements of the original Thomas-Fermi theory) [4–24,43].

In trying to reduce this lack of uniqueness, which mars the beauty of a Thomas-Fermi treatment of average nuclear properties, we decided to use the simplest version of the theory (2 fermions per h^3 of phase space), to restrict to the absolute minimum the number of adjustable parameters in a well-chosen effective interaction, and to pin down these parameters by comparisons with comprehensive sets of data.

The present paper describes the resulting model, together with a number of applications.

2. The Nuclear Thomas-Fermi Model

The model results from a straightforward application of the original theory of Thomas and Fermi (no gradient or exchange corrections!) to a system consisting of two kinds of fermions: neutrons and protons. In addition to the electrostatic interaction between protons, the effective nucleon-nucleon potential is taken to be a Yukawa function of range a . Its strength depends both on the magnitude of the particles' relative momentum p_{12} and on an average of the densities at the locations of the particles. The model is exactly as described in [22]. The

effective interaction v_{12} is thus the Seyler-Blanchard potential of [13], generalized by the addition of one momentum-dependent and one density-dependent term:

$$v_{12} = (2T_0 / \rho_0) \cdot Y(r_{12}) \cdot \left[-\alpha + \beta(p_{12} / P_0)^2 - \gamma(P_0 / p_{12}) + \sigma(2\bar{\rho} / \rho_0)^{2/3} \right] \quad (1)$$

← Seyler-Blanchard attraction with momentum-dependent repulsion →

Additional attraction increases when p_{12} is small (and the two particles would like to become correlated), and tends to zero for large p_{12} , when the particles would zip past each other.

Additional repulsion increases with increasing average density $\bar{\rho}$.

In the above, the quantities T_0 , P_0 , and ρ_0 are the Fermi energy, the Fermi momentum and the particle density of standard nuclear matter, incorporated in Eq. (1) as convenient units, and $Y(r_{12})$ is a normalized Yukawa interaction

$$Y(r_{12}) = \frac{1}{4\pi a^3} \frac{e^{-r_{12}/a}}{r_{12}/a} \quad (2)$$

The average density $\bar{\rho}$ is defined by

$$\bar{\rho}^{2/3} = (\rho_1^{2/3} + \rho_2^{2/3})/2, \quad (3)$$

where ρ_1 and ρ_2 are the relevant densities of the interacting particles (neutrons or protons) at points 1 and 2. The dimensionless interaction strength parameters α , β , γ , σ , may be different for interactions between like and unlike particles. The difference is described by a parameter ξ for the leading (non-saturating) part of the interaction

$$\alpha_{\ell,u} = \frac{1}{2}(1 \mp \xi)\alpha, \quad (4)$$

and by ζ for the saturating parts

$$\begin{aligned}
\beta_{\ell,u} &= \frac{1}{2}(1 \mp \zeta)\beta \\
\gamma_{\ell,u} &= \frac{1}{2}(1 \mp \zeta)\gamma \\
\sigma_{\ell,u} &= \frac{1}{2}(1 \mp \zeta)\sigma ,
\end{aligned} \tag{5}$$

where ℓ,u refer to ‘like’ and ‘unlike,’ and are associated with the minus and plus signs, respectively.

For given neutron and proton densities $\rho_n(\vec{r})$ and $\rho_p(\vec{r})$, the total energy E is a sum of the kinetic energies of the particles E_K , of their nuclear interaction energies E_N , and of the Coulomb energy E_C . The relevant equations are derived in [22], where the reader is referred to for details. They are repeated here for the sake of completeness:

$$E = E_K + E_N + E_C , \tag{6}$$

where

$$E_K / \frac{1}{2} \rho_0 T_0 = \int d^3 r_1 \frac{3}{5} (\Phi_1^5 + \Psi_1^5) , \tag{7}$$

$$\begin{aligned}
E_N / \frac{1}{2} \rho_0 T_0 &= \iint d^3 r_1 d^3 r_2 Y \left\{ \frac{1}{2} \Phi_1^3 \Phi_2^3 \left[-\alpha_\ell + \frac{6}{5} B_\ell \Phi_1^2 - \frac{3}{2} \gamma_\ell \Phi_>^{-1} (1 - \Phi_<^2 / 5 \Phi_>^2) \right] \right. \\
&\quad + \frac{1}{2} \Psi_1^3 \Psi_2^3 \left[-\alpha_\ell + \frac{6}{5} B_\ell \Psi_1^2 - \frac{3}{2} \gamma_\ell \Psi_>^{-1} (1 - \Psi_<^2 / 5 \Psi_>^2) \right] \\
&\quad \left. + \Phi_1^3 \Psi_2^3 \left[-\alpha_u + \frac{3}{5} B_u (\Phi_1^2 + \Psi_1^2) - \frac{3}{2} \gamma_u X_>^{-1} (1 - X_<^2 / 5 X_>^2) \right] \right\} , \tag{8}
\end{aligned}$$

$$E_C = \frac{1}{2} e^2 (\rho_0 / 2)^2 \iint dr_1^3 dr_2^3 \Psi_1^3 \Psi_2^3 / r_{12} , \tag{9}$$

where e is the charge unit and

$$B_{\ell,u} \equiv \beta_{\ell,u} + (5/6) \sigma_{\ell,u} , \tag{10}$$

and, correspondingly,

$$B \equiv \beta + (5/6) \sigma . \tag{11}$$

The following notations were used in Eqs. (7–9):

$$\Phi = \left(\rho_n / \frac{1}{2}\rho_0\right)^{1/3}, \quad \Psi = \left(\rho_p / \frac{1}{2}\rho_0\right)^{1/3} \quad (12)$$

and $\Phi_1, \Phi_2, \Psi_1, \Psi_2$ refer to values of Φ and Ψ at points \bar{r}_1 and \bar{r}_2 . The symbols $\Phi_>, \Phi_<$ stand for “the greater” or “the lesser” of Φ_1 and Φ_2 , and similarly for $\Psi_>$ and $\Psi_<$. The symbols $X_>, X_<$ stand for “the greater” or “the lesser” of Φ and Ψ at \bar{r}_1 and \bar{r}_2 . (See Ref. [22].)

By making the energy E stationary with respect to particle-preserving variations $\delta\rho_n, \delta\rho_p$, one obtains Euler-Lagrange equations for the ground-state neutron and proton density distributions of finite nuclei, of semi-infinite nuclear matter and of uniform infinite nuclear matter. With considerably more effort one can determine the unstable saddle-point configurations for nuclear fission and the associated heights of the fission barriers. The potential felt by a neutron or proton traveling through a nucleus or through nuclear matter, including its energy and isospin dependence, can also be calculated. By comparing the theoretical results with a variety of nuclear data, as described below, we deduced the following values for the seven adjustable parameters of the effective interaction:

$$\begin{aligned} \alpha = 1.94684, & \quad \beta = 0.15311, & \quad \gamma = 1.13672, & \quad \sigma = 1.05 \\ (\because B = 1.02811), & \quad \xi = 0.27976, & \quad \zeta = 0.55665, & \quad a = 0.59294 \text{ fm.} \end{aligned} \quad (13)$$

3. Fitting of Parameters

The calculated Thomas-Fermi binding energies and density distributions depend on six parameters: $\alpha, B, \gamma, \xi, \zeta$ and a (see Eqs. (7–9)). After a number of exploratory studies, the final values of these parameters were determined by an RMS fit to measured binding energies of 1654 nuclei (with neutron and proton numbers $N, Z \geq 8$) together with two geometrical constraints: the radius constant of standard nuclear matter was kept at $r_0 = 1.14$ fm (a value very close to the optimum in the absence of this constraint) and the Süssmann width [25] (diffuseness) of the surface of standard semi-infinite nuclear matter was kept at $b_0 = 1.0$ fm. These two constraints

ensure a close correspondence between calculated and measured charge distributions of finite nuclei, and they leave four effective adjustable freedoms to fit the 1654 binding energies.

The measured binding energies were first corrected as well as possible for three obviously non-smooth contributions, which are outside the framework of a Thomas-Fermi theory. They are the shell effect, the even-odd term and the congruence energy (“Wigner term”) [26]. The result was an almost smooth empirical function of N and Z , to which the Thomas-Fermi model was fitted, yielding (together with the geometrical constraints) the values of α , B , γ , ξ , ζ and a listed in Eq. (13).

Adding to the calculated Thomas-Fermi binding energies, TF, the mass excesses of the neutron and of the Hydrogen atom ($M_n = 8.071431$ MeV, $M_H = 7.289034$ MeV) and the binding energy of the atomic electrons, the predicted atomic mass excess is given by

$$\begin{aligned} \text{Mass excess} = & \text{TF} + M_n N + M_H Z - 0.00001433 Z^{2.39} \\ & + \text{SHELLS} + \text{EVEN-ODD} + G . \end{aligned} \quad (14)$$

The shell correction and the even-odd term were taken from [22] for $N, Z \geq 30$. For $N, Z \leq 29$ we thought it preferable to use the semi-empirical shell corrections from [28] (see Appendix A). The congruence energy G is also patterned after [28] (see Section 9):

$$G = -10 \text{ MeV} \exp(-42|I|/10) , \quad (15)$$

where $I = (N - Z)/A$.

Figure 1 shows the remaining deviations between measurement and theory, with an RMS value of 0.655 MeV.

The seventh adjustable parameter, σ , conveniently decoupled from the first six, was determined by comparing the energy-dependent depths $U(E)$ of optical-model potentials, deduced from neutron and proton scattering experiments, with the Thomas-Fermi formula (Ref. [22]):

$$U(E)/T_0 = -\alpha + \frac{3}{5}\beta + \frac{4}{3}\sigma + \beta\tau - \gamma \begin{cases} \tau^{-1/2} & \text{for } \tau \geq 1 \\ \frac{3}{2} - \frac{1}{2}\tau & \text{for } \tau \leq 1 \end{cases} \quad (16)$$

Here $U(E)$ is the potential felt by a nucleon with kinetic energy τT_0 traveling through standard nuclear matter. The total energy of the nucleon is $E = U + \tau T_0$, which, together with Eq. (16), provides an elementary parametric relation between U and E . This is plotted in Fig. 2 for $\sigma = 1.05$.

4. Properties of Nuclear Matter

The set of parameters in Eq. (13) leads to the following properties of nuclear matter:

- Four Liquid Drop Properties

Radius constant of nuclear matter	$r_0 = 1.14$ fm
Volume binding coefficient	$a_1 = 16.24$ MeV
Symmetry energy coefficient	$J = 32.65$ MeV
Surface energy coefficient	$a_2 = 18.63$ MeV

- Five Droplet Model Properties [26]

Compressibility coefficient	$K = 234$ MeV
Curvature energy coefficient	$a_3 = 12.1$ MeV
Effective surface stiffness coefficient	$Q = 35.4$ MeV
Density symmetry coefficient	$L = 49.9$ MeV
Symmetry anharmonicity coefficient	$M = 7.2$ MeV

For standard nuclear matter with $\rho_n = \rho_p$, the energy per particle as a function of density is given by [22]:

$$\eta(\rho) \equiv \frac{E/A}{T_0} = \frac{3}{5}(1-\gamma)\Omega^2 - \frac{1}{2}\alpha\Omega^3 + \frac{3}{5}B\Omega^3, \quad (17)$$

where $\Omega = (\rho/\rho_0)^{1/3}$ and $\rho_0 = 3/4\pi r_0^3 = 0.16114$ fm⁻³.

Thus

$$E / A = -3.037\Omega^2 - 36.037\Omega^3 + 22.837\Omega^5 \text{ MeV} . \quad (18)$$

For neutron matter the energy per neutron, in units of T_0 , is given by

$$\eta(\rho_n) = \frac{3}{5}(1 - \gamma_\ell)\Phi^2 - \frac{1}{2}\alpha_\ell\Phi^3 + \frac{3}{5}B_\ell\Phi^5 , \quad (19)$$

where $\Phi = (\rho_n / \frac{1}{2}\rho_0)^{1/3}$.

Thus

$$E_n / A = 16.615\Phi^2 - 12.978\Phi^3 + 5.062\Phi^5 \text{ MeV} . \quad (20)$$

This prediction is compared in Fig. 3 with the theoretical estimates of [30], based on very different physical input.

For nuclear matter with a fixed ratio ρ_n/ρ_p , the energy per particle (in units of T_0) is given by (see [22]. Eq. (25)):

$$\eta(\rho) = \frac{3}{5}(1 - \bar{\gamma})\Omega^2 - \frac{1}{2}\bar{\alpha}\Omega^3 + \frac{3}{5}\bar{B}\Omega^5 , \quad (21)$$

where, as before, $\Omega = [(\rho_n + \rho_p)/\rho_0]^{1/3}$, but where the coefficients $\bar{\gamma}$, $\bar{\alpha}$, \bar{B} are now the following functions of the relative neutron excess $I = (\rho_n - \rho_p)/\rho$:

$$1 - \bar{\gamma} = \frac{1}{2}(1 - \gamma_\ell)(p^5 + q^5) - \begin{cases} \frac{1}{4}\gamma_u(5p^2q^3 - q^5) & \text{for } \rho_n \geq \rho_p \\ \frac{1}{4}\gamma_u(5p^3q^2 - p^5) & \text{for } \rho_n \leq \rho_p \end{cases} \quad (22)$$

$$\bar{\alpha} = \frac{1}{2}\alpha_\ell(p^6 + q^6) + \alpha_u p^3 q^3 \quad (23)$$

$$\bar{B} = \frac{1}{2}B_\ell(p^8 + q^8) + \frac{1}{2}B_u p^3 q^3 (p^2 + q^2) , \quad (24)$$

where $p^3 = 1 + I$ and $q^3 = 1 - I$.

Equating to zero the derivative of Eq. (21) with respect to Ω leads to a cubic, which can be readily solved to find algebraic expressions for the equilibrium density, energy and compressibility of nuclear matter with a given neutron excess.

5. Finite Nuclei

Figure 4 shows the calculated charge distributions for ^{56}Fe , ^{124}Sn and ^{209}Bi , compared with Fermi function or “three-parameter gaussian” fits to electron scattering data [31]. Figure 5 shows the neutron and proton density distributions for ^{120}Sn , as well as for ^{167}Sn , the last Thomas-Fermi isotope stable against neutron drip, and ^{83}Sn , the last isotope stable against (non-quantal) proton drip *over* the Coulomb barrier. Figure 6 shows the behaviour of the neutron and proton chemical potentials for isotopes between these extremes.

Figure 7 shows the last unruptured nucleus and the first bubble nucleus [32] in a sequence of solutions (constrained to spherical symmetry) for which $(N - Z)/A$ was fixed at 0.2 and A was increased in steps of 10 (up to $A = 1000$). The rupture or cavitation into a bubble occurs at about $Z^2/A \approx 100$, as expected on the basis of a liquid drop model [33, 34].

Altogether we calculated the binding energies of some 9,000 nuclei, both neutron- and proton-rich, as well as super-heavy. Out of curiosity we also calculated the binding energies (with shell, even-odd and congruence energies added) for nuclei with $N, Z < 8$, expecting a macroscopic-microscopic treatment to break down completely for such small mass numbers. To our surprise we found that the deviations between theory and measurement were not much greater in this region than for somewhat heavier nuclei included in the RMS fit. The binding energy of the alpha particle came out to be -29.80 MeV instead of -28.30 MeV, an error of 1.5 MeV. For $A = 3(!)$, ^3He was bound by 7.27 MeV instead of 7.72 MeV, and tritium by 8.25 MeV instead of 8.48 MeV. For $A = 2(!)$, the deuteron was found to be unbound by 2.6 MeV instead of being bound by 2.2 MeV.

In the heavy and super-heavy region, the extrapolated mass defect of ^{264}Hs ($Z = 108$), not included in our RMS fit, comes out as 120.28 MeV, compared with the experimental value

119.82 ± 0.30 MeV. Figure 8 gives a sample of the mass defects in this region of the periodic table.

6. Fission Barriers

Using the techniques described in [23] we calculated 45 Thomas-Fermi fission barriers ranging from ^{252}Cf down to ^8Be . In order to compare theory with measured values, listed in Fig. 9, one must decide how the non-smooth contributions to the energy (shell, even-odd, congruence) change in going from the ground state shape to the saddle-point shape. Figures 10–12 are based on the following illustrative assumptions: (i) the ground-state shell effect disappears at the saddle, (ii) the odd-even term does not change appreciably, (iii) the congruence energy does not change in the case of heavy elements, when the saddle shape is not necked in, but (iv) doubles its original value for light elements, when the saddle shape is highly necked in.

For the heaviest elements in Fig. 10 (with $Z = 88, 90, 92, 94, 96, 98$) the agreement between measurement and theory (upper curve) is almost perfect, even though no parameters were re-adjusted after the fit to ground-state masses. For the lighter elements in Fig. 10 a systematic deviation from the upper curve based on assumption (iii) comes in, and the measurements seem to approach the lower curve, based on assumption (iv). This trend begins at about the point where the saddle shapes have developed a pronounced neck, suggesting that the congruence energy is beginning to increase as the neck constriction develops. The four barrier measurements for the lightest nuclei, $^{90,94,98}\text{Mo}$ and ^{75}Br [42], would seem to reinforce this hypothesis (Fig. 11). Assuming that for these strongly necked-in saddles the congruence energy has doubled, the predicted barriers are fairly close to the measurements, whereas without this assumption the barriers for the above nuclei would be overestimated by about 7–10 MeV. Note also that for ^8Be the doubling of the congruence energy reduces the calculated barrier from about 13 MeV to about 3 MeV, a value more nearly consistent with the observed instability of ^8Be against fission into two alpha particles. This is indicated by an experimental point at 2.3 MeV, the formal “empirical” ground state shell effect of ^8Be (see below).

Figure 11 shows a blow-up of the calculated and measured barriers for $Z = 90$ to 98 . A systematic overestimate of about 0.5 MeV can be seen. At this level of precision a number of effects might be responsible for the differences. (Shell effects, experimental uncertainties, further fine tuning of adjustable parameters...?)

Concerning the experimental points plotted in Figs. 10–12, they were obtained by adding to the measured ground-state mass of a given nucleus its measured fission barrier (thus obtaining a *measured* saddle-point mass) and plotting the results with respect to smooth calculated Thomas-Fermi ground state masses (with the appropriate even-odd term included, but *without* the theoretical ground state shell correction). Because the resulting measured saddle point masses (solid diamonds in Fig. 10) deviate from a smooth trend by no more than about 1 MeV, it can be concluded that, as expected, saddle-point masses exhibit relatively small shell corrections. Similarly, the absence of pronounced staggering between points for even-even and odd- A nuclei sets an upper limit on the *change* in the even-odd correction in going from the ground state to the saddle.

7. Surface Energy and Compressibility

As noted in [22], if the compressibility coefficient K is plotted vs. the surface energy coefficient a_2 for a fixed value of the surface diffuseness, an amazingly linear relation is found. Figure 13 shows this relation for the present set of parameters. It can be represented very accurately by

$$a_2 = 1.5 + [0.063011 + 0.06682(b_0 - 1)](K + 38) \quad , \quad (25)$$

where b_0 is in fm and a_2 and K are in MeV.

According to this equation a relative change $\delta b_0/b_0$ in the assumed width away from $b_0 = 1$ fm produces a relative change $\delta K/K$ equal to $-1.23 \delta b_0/b_0$. Thus $b_0 = 1.05$ fm would give $K = 220$ MeV and $b_0 = 0.95$ fm would give $K = 249$ MeV.

Equation (25) may also be useful for estimating K for other versions of the model. Thus, for the set of parameters used in [22] ($a_2 = 20.268$ MeV, $b_0 = 0.8713$ fm—not an optimal choice), Eq. (25) implies $K = 306.93$ MeV, which is within 2% of the 301.25 MeV of [22].

8. The Curvature Energy Puzzle

References [35, 36] discussed an apparent difficulty in reconciling theoretical calculations, which invariably lead to a curvature energy coefficient a_3 of about 10 MeV, with empirical fits to nuclear binding energies, which were believed to require $a_3 \approx 0$. Our Thomas-Fermi model is characterized by $a_3 = 12.1$ MeV, but has no difficulty in fitting binding energies. As discussed in [37] the reason for the original puzzle is, we believe, that terms of still higher order in $A^{-1/3}$ tend to counteract the curvature correction and, if not allowed for explicitly, mask its presence. As an illustration of this effect suppose that the true binding energy, in MeV, for $N = Z$ nuclei (without Coulomb and microscopic corrections) could be approximated by

$$E = -16.24 A + 18.63 A^{2/3} + 9.15 A^{1/3} - 11.54 ,$$

where the first three coefficients correspond to our Thomas-Fermi model and the last one, representing higher-order terms, is chosen, as in [37] to make the binding vanish at $A = 1$. (The number 9.15 is equal to the quantity $(a_3 - 2a_2^2/K)$, which is the Thomas-Fermi prediction for the coefficient of $A^{1/3}$). An RMS fit to Eq. (26), in the range $A = 15$ to $A = 240$, of an expression without the last term, viz.,

$$\bar{E} = -\bar{a}_1 A + \bar{a}_2 A^{2/3} + \bar{c}_3 A^{1/3} \tag{27}$$

gives

$$\bar{a}_1 = 16.3294,$$

$$\bar{a}_2 = 20.0280,$$

$$\bar{c}_3 = 2.067 .$$

The RMS deviation between Eq. (26) and Eq. (27) is only 0.16 MeV! Thus, by increasing a_1 slightly, a_2 significantly (by 1.4 MeV) and by *decreasing the coefficient of $A^{1/3}$ to a value close to zero*, one can mock up the missing higher-order term with excellent accuracy, and mask in this way the presence of a curvature correction.

In any case, since our Thomas-Fermi model has a curvature correction of 12.1 MeV and gives a good fit to masses, the curvature correction puzzle seems to have been disposed of.

9. Suggested Interpretation of the Congruence Energy

In the Thomas-Fermi treatment one evaluates the interaction energy between the fermions as if they constituted a structureless, homogenized fluid. In fact, the density of a quantized nucleon in a mean-field potential well consists of cushion-like bumps, boxed in by a three-dimensional lattice of nodal surfaces. The interaction energy between two fermions with such modulated, granular density distributions will obviously be somewhat greater—in the case of short-range forces—when the two interacting densities have identical (congruent) nodal structures, compared to the case of two uncorrelated densities. As a qualitative illustration of the possible implications of this extra interaction, imagine A originally independent nucleons in a mean-field potential, filling the lowest energy states in the usual four independent sub-groups: N neutrons and Z protons with spins up and down. (Spin-orbit and Coulomb forces are disregarded.) An elementary calculation, sketched in Fig. 14, shows that the formula for the number of nucleon pairs with identical spatial wave functions consists of a leading term proportional to A , modified by an even-odd term independent of A , and reduced further by a term of the form

$$-A|I|, \quad (28)$$

where $I = (N - Z)/A$. (The even-odd term includes a contribution δ , where $\delta = 1$ for $N = Z = \text{odd}$, and zero otherwise.)

The interaction energy between a pair of nucleons interacting by short-range forces is inversely proportional to the volume—itsself approximately proportional to A —in which the nucleons are confined. It follows that the extra binding associated with the presence of congruent pairs will consist of a negative contribution independent of A , an even-odd correction (including the term δ/A) proportional to A^{-1} , and a further positive correction proportional to $|I|$. In [28] we used the expression

$$\begin{aligned} G &= -7\text{MeV} \exp(-6|I|) \\ &\approx -7 + 42|I| + \dots \text{ MeV, for small } I, \end{aligned} \tag{29}$$

to represent the congruence energy (apart from the even-odd correction). The exponential form of Eq. (29) prevents G from becoming positive, which would violate the physical requirement that the congruence energy should represent an extra *binding*. (This is in contrast to an expression simply proportional to $|I|$.)

The value of the derivative $dG/d|I|$, approximately equal to 42 MeV for small I , is suggested directly by the half-angle of the empirically observed V-shaped binding energy trough around $N = Z$. The pre-exponential coefficient -7 MeV is much more uncertain. In the final stages of our current fits to masses we allowed both the amplitude and the range in Eq. (29) to vary, along with the other four effective freedoms in the adjustable parameters (resulting in a search in a six-parameter space). It turned out that the optimum half-angle of the trough was indeed close to 42 MeV. The optimum value of the pre-exponential term was close to -10 MeV. We consequently adopted for the congruence energy the expression given by Eq. (15).

The nature of the shape dependence of the congruence energy is an outstanding unsolved problem. The extra binding in question reflects in the first place the number of congruent pairs, and this depends only on the partition—*independent of shape*—of the nucleons into the four classes: neutrons and protons with spin up and down. The congruence energy might then be independent of shape in some average sense. (In the case of the box potential in [26], this independence from the box's shape is, in fact, exact in the limit of zero-range forces.) But the

shape independence needs one curious topological qualification. When a system divides into two pieces, each fragment will have—according to our analysis—a congruence energy independent of its mass number, and equal to the original congruence energy. Hence the total congruence energy will have doubled. This doubling may actually be traced to the circumstance that two originally congruent nucleons in a dividing potential well will (almost always) both end up *either* in one fragment *or* the other. (Exceptional cases in which a wave function ends up with comparable amplitudes in two well separated fragments have negligible probability.) The two nucleons will then be exploring a smaller volume and interacting more strongly than before. But how, precisely, the doubling of the congruence energy proceeds as the communication between the two nascent fragments is suppressed, appears to be an open question.

The above qualitative considerations, embodied in the semi-empirical Eq. (15), have led us to believe that the binding energy trough around $N = Z$ is, to an appreciable extent, a reflection of the granularity of the nucleonic densities, and that a refined analysis of fission barrier trends provides evidence for the topological doubling of this congruence energy.

10. Concluding Remarks

The overall conclusion of this work is simply stated: Applying the 1927 statistical method of Thomas and Fermi to nuclei, it is possible to construct a model which reproduces closely a wide range of nuclear properties.

The effective nucleon-nucleon interaction necessary to achieve this is found to depend on the particles' relative momentum p_{12} as well as on the density surrounding the particles. The momentum dependence is found to be mostly of the p_{12}^{-1} kind, with a smaller admixture of a term proportional to p_{12}^2 .

After adding shell and even-odd corrections, as well as a semi-empirical congruence energy, it is possible to reproduce 1,654 nuclear ground state masses to within an RMS deviation of 0.655 MeV for $N, Z \geq 8$.

Having fitted six adjustable parameters of the effective interaction to ground state masses and the surface diffuseness, the nuclear RMS radii and the fission barriers of heavy nuclei come out very close to measurements without further parameter adjustments. The trend of the fission barriers for elements below about $Z = 88$ may be interpreted as evidence for the expected tendency of the congruence energy to double its value as the neck in the saddle-point shapes tends to zero. If this interpretation is confirmed, it will lend weight to the hypothesis that the term in nuclear binding energies proportional to $|N - Z|/A$ arises to a significant extent from the stronger interaction between 'congruent' nucleons, characterized by similar nodal structures of their wave functions.

With the nuclear Thomas-Fermi model firmly anchored in a large body of experimental data, we expect it to be relatively reliable for extrapolating to various extreme situations, such as nuclear and neutron matter, nuclei near the drip lines, as well as superheavy nuclei, including bubble and other exotic geometries. Soon we hope to subject our Thomas-Fermi nuclei to large centrifugal forces and, eventually, to high temperatures.

Acknowledgments

We would like to thank P. Möller and J.R. Nix for stimulating discussions extending over many years, and for help with accessing data on nuclear masses, shell effects and even-odd corrections. We are grateful to L.G. Moretto, K. Jing and G. Wozniak for providing us with their recent results on the fission barriers of $^{90,94,98}\text{Mo}$ and ^{75}Br .

This work was supported in part by the Director, Office of Energy Research, Office of High Energy and Nuclear Physics, Division of Nuclear Physics, and by the Office of Basic Energy Sciences, Division of Nuclear Sciences, of the U.S. Department of Energy under Contract No. DE-AC03-76SF00098.

Appendix A

Shell and Even-Odd Terms

For $N, Z \geq 30$ we took the shell effect from [27], column headed E_{mic} . These estimates, based on the Strutinsky shell-correction method, become unreliable for light nuclei, and are not available for the lightest, with $N, Z < 8$. Accordingly, for $N, Z \leq 29$ we used semi-empirical shell corrections $S(N, Z)$ based on [28]:

$$S(N, Z) = \frac{1}{2} [N^{2/3} S(N) + Z^{2/3} S(Z)] / (A/2)^{2/3}, \quad (\text{A.1})$$

where $S(X)$ is listed in Table I.

For the even-odd term we used for all values of N and Z the expressions from [27] (incorporating in this term the correction $30 \text{ MeV}/A$, which is listed as part of the “Wigner energy” in that reference). Thus:

$$\text{Even - Odd (in MeV)} \left\{ \begin{array}{ll} \frac{4.8}{N^{1/3}} + \frac{4.8}{Z^{1/3}} - \frac{6.6}{A^{2/3}} + \frac{30}{A}, & N = Z, \text{ odd} \\ \frac{4.8}{N^{1/3}} + \frac{4.8}{Z^{1/3}} - \frac{6.6}{A^{2/3}}, & N \text{ and } Z \text{ odd} \\ \frac{4.8}{Z^{1/3}}, & N \text{ even, } Z \text{ odd} \\ \frac{4.8}{N^{1/3}}, & N \text{ odd, } Z \text{ even} \\ 0, & N \text{ and } Z \text{ even} \end{array} \right. \quad (\text{A.2})$$

Table I. Shell function derived from the masses of nuclei with equal numbers of neutrons and protons [28].

Particle number X	$S(X)$ (MeV)	Particle number X	$S(X)$ (MeV)	Particle number X	$S(X)$ (MeV)
1	-1.779	11	2.835	21	3.240
2	-1.506	12	1.640	22	3.230
3	0.238	13	1.895	23	2.583
4	0.709	14	-0.261	24	1.698
5	2.364	15	-0.231	25	0.770
6	-0.693	16	0.656	26	-0.160
7	-1.329	17	1.053	27	-1.305
8	-0.449	18	1.568	28	-2.846
9	2.714	19	1.872	29	-2.214
10	2.807	20	1.707		

Appendix B

Fission Barriers

The fission barriers in Fig. 9 were calculated as in [23], by solving the Thomas-Fermi Euler-Lagrange equilibrium equations for a density distribution constrained to have a prescribed separation between the centers of mass of its two reflection symmetric halves. By increasing the prescribed separation in small steps away from the sphere one can trace out a deformation energy curve along a “fission valley,” whose maximum, if it exists, defines the fission barrier for the nucleus in question. In practice, this works for nuclei down to about $Z = 70-75$, but for lighter systems the constrained Thomas-Fermi solutions cease to exist at a point where the deformation energy is still on the increase, and the fission barrier cannot be deduced from such a plot.

There do exist solutions to the Thomas-Fermi equations for larger deformations, but they correspond to two separated fragments, whose centers of mass are held at the prescribed separation. Decreasing the constraining distance along this family of shapes traces out the energy along the “fusion valley” but, except for the lightest systems, the solutions again terminate before a maximum has been reached. This phenomenon, an example of a “catastrophe” [38], is associated with the fact that saddle point shapes, when arranged according to a deformation constraint of the type of a distance between centers of mass, or a quadrupole moment, trace out in deformation space an S-shaped curve. The top of the S corresponds, let us say, to the fission valley, the bottom to the fusion valley, and the middle, between the two bends, to a potential energy ridge between the two “misaligned” valleys [39]. For a range of intermediate mass nuclei, the saddle point is on this ridge, and in those cases the energy is a minimum with respect to the constraining parameter, the saddle point’s instability being manifested in one of the other degrees of freedom. The result is that the constrained Thomas-Fermi Euler-Lagrange equations are now asked to find a solution that is no longer a minimum in all the degrees of freedom that are being varied. And this, apparently, they refuse to do.

We have found a way around this difficulty by the following stratagem. Consider the deformation energy $V(\alpha, \theta)$ to be a function of a constraining parameter θ and of the other deformation degrees of freedom, represented collectively by α . Write down an expression for $V(\alpha, \theta)$ which interpolates the deformation energy on the inaccessible ridge, between the two bends in the S-curve. The simplest such expression is linear in θ and quartic in α . (A quartic is called for by the requirement that the vanishing of the partial derivative of V with respect to α should give an S-shaped cubic for the dependence of θ on α .) This interpolating function may be reduced to the form

$$V(\alpha, \theta) = V_0 - B\theta + \alpha\theta - \frac{1}{2}a\alpha^2 + \frac{1}{12}b\alpha^4, \quad (\text{B.1})$$

where V_0 , B , a and b are four parameters to be determined by matching to known properties of the deformation energy at the last accessible points along the fission and fusion valleys. The algebraic manipulations are explained below, but having determined V_0 , B , a , b one may now locate by differentiations the saddle point in the deformation energy, Eq. (B.1), with the following result for the fission barrier energy V_{SP} :

$$V_{\text{SP}} = \bar{V} - (\bar{V} - V_x) \left(\frac{3}{8} + 3\beta^2 - 2\beta^4 \right), \quad (\text{B.2})$$

where

$$\beta = \Delta V / 4(\bar{V} - V_x),$$

$$\bar{V} = (V_A + V_B) / 2 = \text{average of } V_A \text{ and } V_B, \text{ the energies at the last accessible (limiting) points in the fusion and fission valleys, respectively,}$$

$$\Delta V = V_B - V_A,$$

$$V_x = \text{energy of the intersection point of the tangents drawn at the two limiting points A and B, as illustrated in Fig. 15.}$$

Proof:

The locus of constrained (conditional) equilibrium shapes is given by

$$\left. \frac{\partial V}{\partial \alpha} \right|_{\theta} = \theta - a\alpha + \frac{1}{3}b\alpha^3 = 0 \quad , \quad (\text{B.3})$$

i.e.,
$$\theta(\alpha) = a\alpha - \frac{1}{3}b\alpha^3 \quad . \quad (\text{B.4})$$

The turning (limiting) points in this S-curve are given by $d\theta/d\alpha = 0$, i.e., by

$$\alpha_{A,B} = \mp \sqrt{a/b} \quad , \quad \theta_{A,B} = \mp 2a^{3/2}/3\sqrt{b} \quad . \quad (\text{B.5})$$

The energies at these points are

$$V_{A,B} = V_0 \pm \frac{2}{3}B \frac{a^{3/2}}{\sqrt{b}} + \frac{1}{4} \frac{a^2}{b} \quad . \quad (\text{B.6})$$

The derivatives at A and B, defined by

$$\frac{dV(\alpha(\theta), \theta)}{d\theta} = \frac{\partial V}{\partial \alpha} \frac{d\alpha}{d\theta} + \frac{\partial V}{\partial \theta} = \frac{\partial V}{\partial \theta}$$

and denoted by $V'_{A,B}$, are found to be given by

$$V'_{A,B} = -B + \alpha_{A,B} \quad . \quad (\text{B.7})$$

Relations (B.6) and (B.7) represent four equations for V_0 , B , a , b , whose solution gives

$$V_0 = \bar{V} - (3/32)\Delta V \Delta V' / \bar{V}' \quad (\text{B.8})$$

$$B = -\bar{V}' \quad (\text{B.9})$$

$$a = (3/2)\Delta V / \Delta V' \bar{V}' \quad (\text{B.10})$$

$$b = 6\Delta V / \bar{V}' (\Delta V')^3 \quad , \quad (\text{B.11})$$

where

$$\bar{V}' = \frac{1}{2}(V'_A + V'_B) \quad \text{and} \quad \Delta V' = V'_B - V'_A \quad . \quad (\text{B.12})$$

Finally, a straight line with value V_A and slope V'_A at A, and a line with value V_B and slope V'_B at B (the distance from A to B being $2\theta_B = 4a^{3/2}/3\sqrt{b} = \Delta V/\bar{V}'$ by Eqs. (B.10, B.11)) are readily shown to intersect at a point whose energy is

$$V_x = \bar{V} - \Delta V \Delta V' / 4 \bar{V}' . \quad (\text{B.13})$$

(The location of this point is at $\theta = 0$.)

By differentiating Eq. (B.1) the location of the saddle point is found to be

$$\alpha_{\text{SP}} = B \quad , \quad \theta_{\text{SP}} = aB - \frac{1}{3}bB^3 . \quad (\text{B.14})$$

Inserting in Eq. (B.1) and making use of Eqs. (B.8–B.11, B.13) yields Eq. (B.2).

The location of the saddle point itself may be written in the form

$$\theta_{\text{SP}} = \frac{1}{2}(\theta_A + \theta_B) + \left(-\frac{3}{2}\beta + 2\beta^3\right)(\theta_B - \theta_A) . \quad (\text{B.15})$$

More generally, if the deformation energy is plotted, as in our calculations, against a constraining parameter Δ related to θ by a change of origin, the equation for Δ_{SP} is

$$\Delta_{\text{SP}} = \frac{1}{2}(\Delta_A + \Delta_B) + \left(-\frac{3}{2}\beta + 2\beta^3\right)(\Delta_B - \Delta_A) . \quad (\text{B.16})$$

Figure 13 illustrates these constructions in the case of the nucleus with $Z = 42$, $N = 56$.

REFERENCES

1. L. H. Thomas, Proc. Cambridge Phil. Soc. **33** (1927) 542
2. E. Fermi, Rend. Lincei **6**, (1927) 602; Zeit. f. Physik **48** (1928) 73
3. P. Gombas, "Die statistische Theorie des Atoms und ihre Anwendung" (Springer, Wien, 1949).
4. M. Brack, C. Guet and H.-B. Hakansson, Phys. Rep. **123** (1985) 275
5. K. A. Brueckner, J. H. Chirico and H. W. Meldner, Phys. Rev. C **4** (1971) 732
6. A. K. Dutta, J.-P. Arcoragi, J. M. Pearson, R. Behrman and F. Tondeur, Nucl. Phys. A **458** (1986) 77
7. F. Tondeur, A. K. Dutta, J. M. Pearson and R. Behrman, Nucl. Phys. A **470** (1987) 93
8. J. M. Pearson, Y. Aboussir, A. K. Dutta, R. C. Nayak, M. Farine and F. Tondeur, Nucl. Phys. A **528** (1991) 1
9. Y. Aboussir, J. M. Pearson, A. K. Dutta and F. Tondeur, Nucl. Phys. A **549** (1992) 155
10. F. Garcias, M. Barranco, J. Nemeth and C. Ngô, Phys. Lett. B **206** (1988) 177
11. F. Garcias, M. Barranco, J. Nemeth, C. Ngô and X. Viñas, Nucl. Phys. A **495** (1989) 169
12. P. Ring and P. Schuck, "Nuclear Many Body Problem," Springer-Verlag, New York/Berlin, 1980.
13. R. G. Seyler and C. H. Blanchard, Phys. Rev. **124**, (1961) 227; **131** (1963) 355
14. D. Von-Eiff, S. Haddad and M. K. Weigel, Phys. Rev. **C50** (1994) 1244
15. M. M. Sharma, M. A. Nagarajan and P. Ring, Ann. of Phys. **231** (1994) 110
16. M. M. Majumdar, S. K. Samaddar, N. Rudra and J. N. De, Phys. Rev. **C49** (1994) 541
17. M. Centelles, X. Viñas, M. Barranco, N. Ohtsuka, A. Faessler, D. T. Khoa and H. Müther, Phys. Rev. **C47** (1993) 1091
18. P. Gleissl, M. Brack, J. Meyer and P. Quentin, Ann. of Phys. **197** (1990) 205
19. F. Garcias, M. Barranco, A. Faessler and N. Ohtsuka, Zeit. f. Physik **A336** (1990) 31
20. D. Bandyopadhyay and S. K. Samaddar, Nucl. Phys. A **484** (1988) 315

21. W. D. Myers and W. J. Swiatecki, *Ann. Phys. (N.Y.)* **55** (1969) 395
22. W. D. Myers and W. J. Swiatecki, *Ann. Phys. (N.Y.)* **204** (1990) 401
23. W. D. Myers and W. J. Swiatecki, *Ann. Phys. (N.Y.)* **211** (1991) 292
24. W. J. Swiatecki, *Acta Physica Polonica* **B24** (1993) 229
25. R. W. Hasse and W. D. Myers, "Geometrical Relationships of Macroscopic Nuclear Physics," Springer-Verlag, New York/Berlin, 1988
26. W. D. Myers, "Droplet Model of Atomic Nuclei," IFI/Plenum, New York, 1977
27. P. Möller, J. R. Nix, W. D. Myers and W. J. Swiatecki, "Nuclear Ground State Masses and Deformations," Los Alamos preprint LA-UR-93-3083, Aug. 16, 1993, to be published in the *Atomic Data and Nuclear Data Tables*
28. W. D. Myers and W. J. Swiatecki, *Nucl. Phys.* **81** (1966) 1
29. M. Bauer, E. Hernández-Saldaña, P. E. Hodgson and J. Quintanilla, *J. Phys. G: Nucl. Phys.* **8** (1982) 525
30. B. Friedman and V. R. Pandharipande, *Nucl. Phys.* **361**(1981) 502
31. H. de Vries, C. W. Jager and C. de Vries, *At. Data Nucl. Data Tables* **36** (1987) 495
32. W. D. Myers and W. J. Swiatecki, "The Nuclear Thomas-Fermi Model," Lawrence Berkeley Laboratory preprint LBL-36004, Aug. 1994, to be published in *Proc. XXIX Zakopane School of Physics, Zakopane, Poland, Sept. 5–14, 1994*, in *Acta Physica Polonica*
33. W. J. Swiatecki, Ph.D. Thesis, University of Birmingham, October 1949
34. W. J. Swiatecki, *Physica Scripta* **28** (1983) 349
35. W. Stocker, J. Bartel, J. R. Nix and A. J. Sierk, *Nucl. Phys.* **A489** (1988) 252
36. M. Durand, P. Schuck and X. Viñas, *Zeit. f. Physik* **A346** (1993) 87
37. W. D. Myers and W. J. Swiatecki, "Thomas-Fermi Treatment of Nuclear Masses, Deformations and Density Distributions," Lawrence Berkeley Laboratory preprint LBL-36005, Aug. 1994, to be published in *Proc. Fourth KINR International School on Nuclear Physics, Kiev, Ukraine, Aug. 29–Sept. 7, 1994*

38. R. Gilmore, "Catastrophe Theory for Scientists and Engineers," Dover Publ. Inc., New York, 1981
39. W. J. Swiatecki, *Journal de Physique* **33** (1972) C5
40. L. G. Moretto, S. G. Thompson, J. Routti and R. C. Gatti, *Phys. Lett.* **38B** (1972) 471
41. H. C. Britt, Proc. 4th IAEA Symposium on the Physics and Chemistry of Fission, Jülich 1979, Vol. 1, p. 3, IAEA Vienna, 1980
42. L. G. Moretto, K. Jing and G. Wozniak, Lawrence Berkeley Laboratory preprint LBL-36186, 1994; K. Jing and G. Wozniak, private communication, May 1994.
43. J. Randrup and E. de Lima Medeiros, *Nucl. Phys.* **A529** (1991) 115; *Phys. Rev.* **C45** (1992) 372.

FIGURE CAPTIONS

- Fig. 1. The difference: (measured mass) minus (theoretical mass) for 1654 nuclei. Lines connect isotopes. Upper panel based on [27], lower panel on the present model.
- Fig. 2. The compilation of measured optical model potential depths (corrected for Coulomb effects and neutron excess [29]) is compared with the Thomas-Fermi formula, Eq. (16).
- Fig. 3. The energy per particle of neutron matter as a function of the cube root of the neutron density relative to its value in standard nuclear matter, as given by $\Phi = (\rho_n / \frac{1}{2} \rho_0)^{1/3}$. The curve is the Thomas-Fermi result, Eq. (20), the squares are theoretical predictions from [30].
- Fig. 4. The Thomas-Fermi charge distributions for ^{56}Fe , ^{124}Sn and ^{209}Bi (solid lines) are compared with electron scattering measurements, as represented by fits to the data using a Woods-Saxon function (dot-dashed) or a “three-parameter gaussian” (dashed) [31].
- Fig. 5. The neutron (solid lines) and proton (dashed lines) density distributions for ^{83}Sn , ^{120}Sn and ^{167}Sn , according to the Thomas-Fermi model. Here and in Fig. 4 a nucleon Yukawa form factor with an RMS size of 0.85 fm has been folded in.
- Fig. 6. Neutron (open squares) and proton (solid squares) Thomas-Fermi chemical potentials for isotopes from ^{83}Sn to ^{167}Sn .
- Fig. 7. The last unruptured nucleus ($N = 372$, $Z = 248$) and the first bubble nucleus ($N = 378$, $Z = 252$) in a sequence where A was increased in steps of 10 while $(N-Z)/A$ was held fixed at the value 0.2. Here the parameters of the effective interaction were taken from [22].
- Fig. 8. The Thomas-Fermi mass excess without the shell correction (upper entry) and the shell correction from [27] (lower entry), for heavy and super-heavy nuclei, tabulated against Z and $N-Z$. The entries in parentheses refer to extremely deformed shapes with minuscule barriers against fission.

Fig. 9. A compilation of fission barriers. The fourth column is "Fissility," defined as $Z^2/A(1 - 2.2I^2)$. The fifth column gives experimental fission barriers from [40–42]. "Shell" is (experimental mass) less (theoretical mass with all corrections except the theoretical shell correction). "Congr" is the congruence energy. TF Lower and TF Upper are the Thomas-Fermi fission barriers calculated assuming that the congruence energy has doubled at the saddle point or that it remained unchanged. "Saddle," equal to "Exp. Barr" plus "Shell," is the quantity to be compared with the adjoining theoretical predictions.

Fig. 10. Calculated fission barriers (open symbols) and measurements corrected for ground-state shell effects (solid diamonds). The open diamonds are based on the assumption that the congruence energy at the saddle point is the same as in the ground state, the open squares assume that it has doubled. "Fissility" is defined as $Z^2/A(1 - 2.2I^2)$, where the factor 2.2 was adjusted so as to make the calculated points follow approximately a single curve in the region of the heavy elements.

Fig. 11. Same as Fig. 10 but extended down to ^8Be . The four points around fissility 16–19 refer to $^{90,94,98}\text{Mo}$ and ^{75}Br [42]. The other experimental points are from [40–41].

Fig. 12. Same as Figs. 10, 11 but for the heaviest nuclei: Th, U, Pu, Cm and Cf.

Fig. 13. Each set of symbols represents the result of calculating the compressibility of nuclear matter with parameters that result in the indicated surface width b_0 and surface energy coefficient a_2 . (The energy per particle and the radius constant of nuclear matter are kept fixed at $a_1 = 16.24$ MeV, $r_0 = 1.14$ fm.) The circle indicates the optimum fit parameters.

Fig. 14. Partitions of N,Z nucleons with spin up/down into four groups, and the counting of identical pairs in four different situations: even-even, odd-A, odd-odd and odd-odd with $N = Z$.

Fig. 15. The equilibrium deformation energy for a reflection and axially symmetric ^{98}Mo nucleus, constrained to have the centers of mass of its two halves at a separation

exceeding by Δ the separation for the spherical ground-state configuration. The circles follow the fission valley up to the limiting point B. The triangles follow the fusion valley down to the limiting point A. The tangents at A and B cross at X, and Eq. (B.2) in the text gives the saddle-point energy V_{SP} in terms of the energies at A, B, and X.

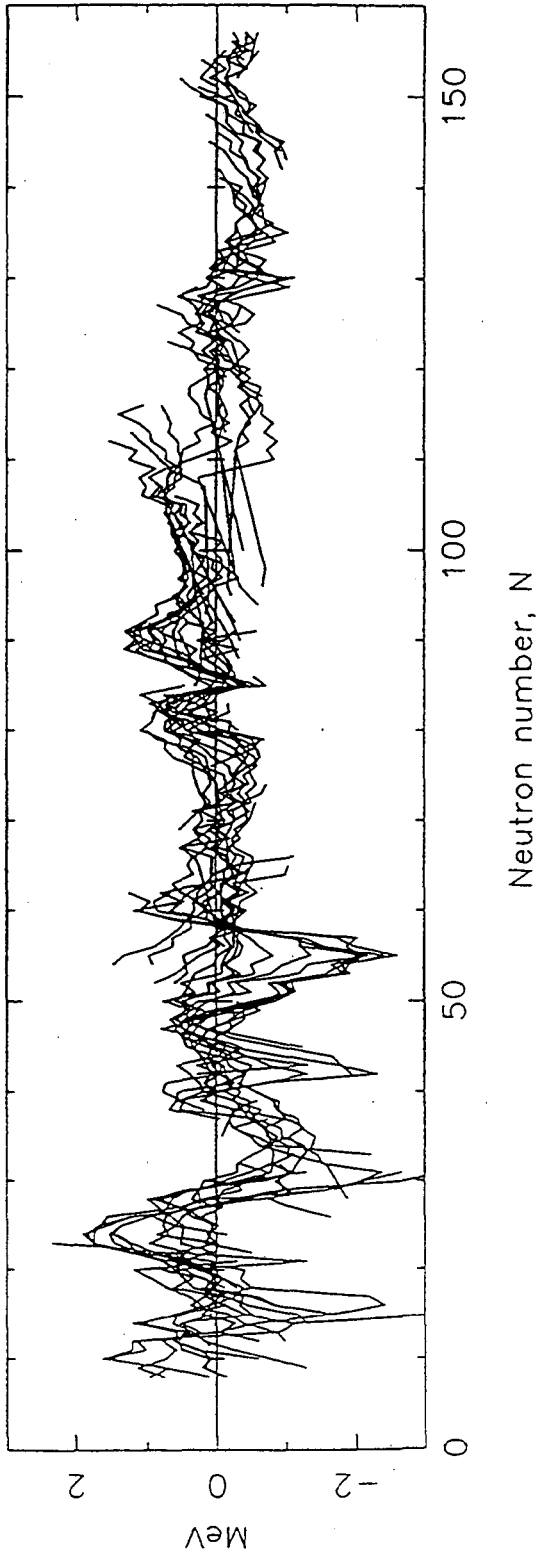
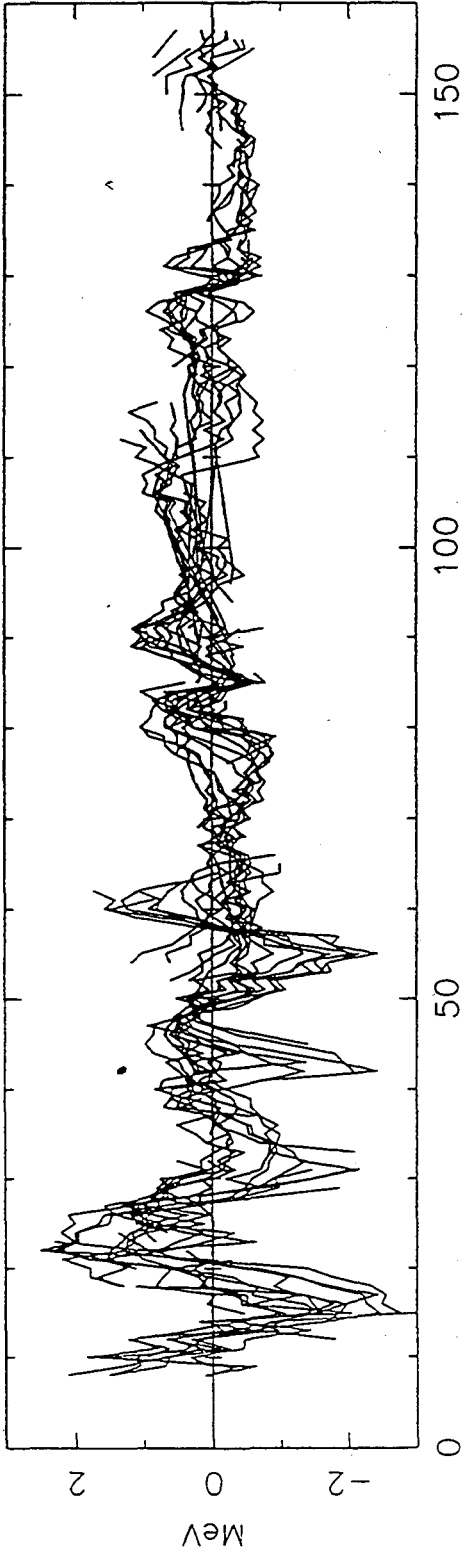


Figure 1

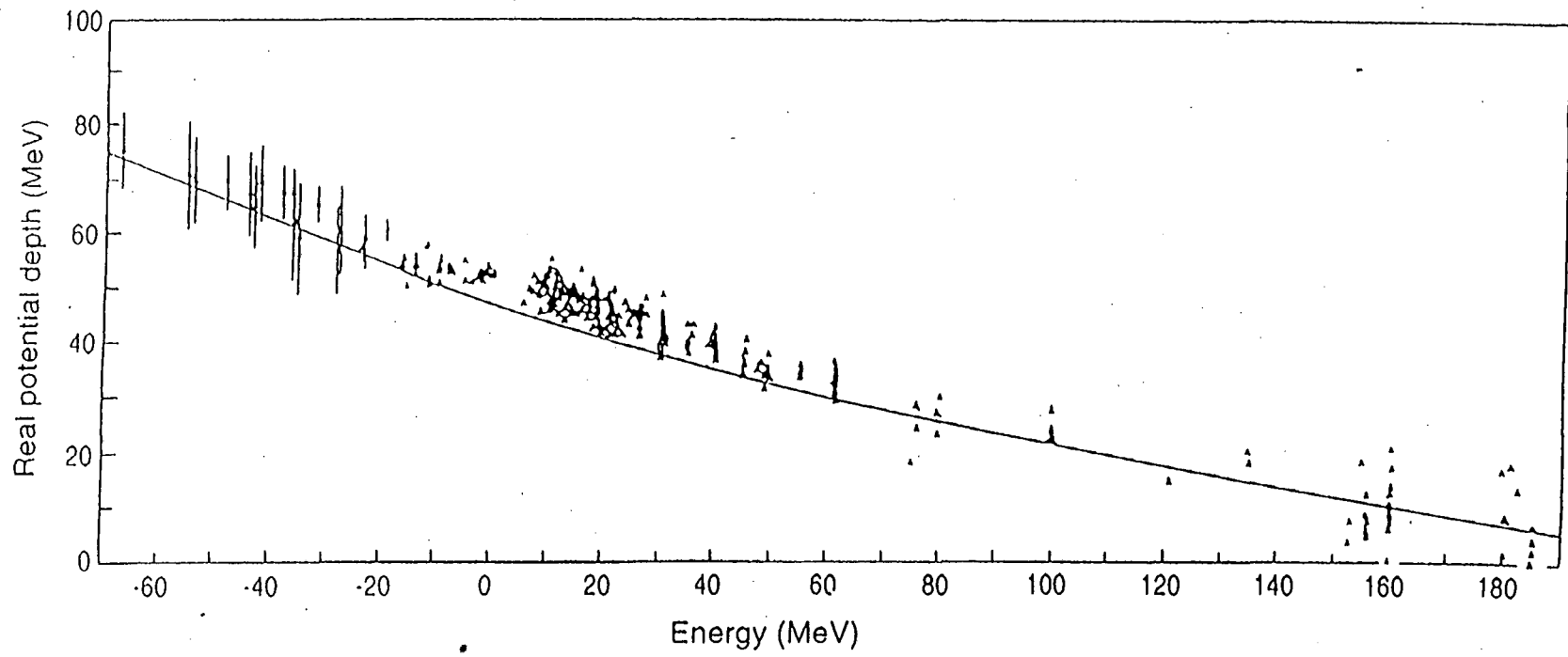


Figure 2

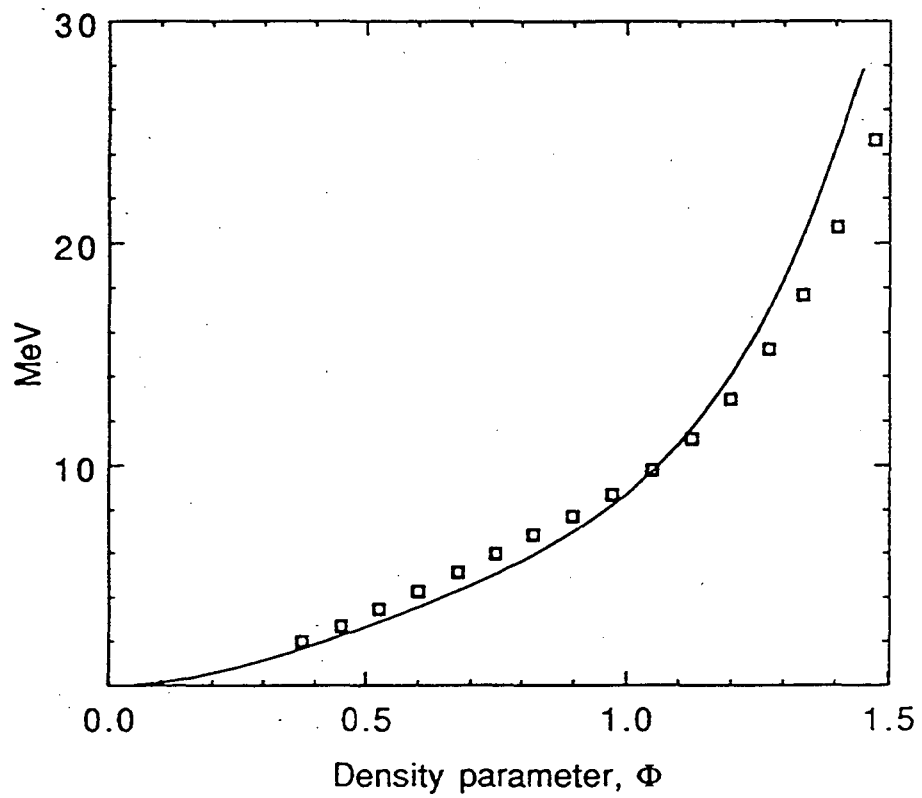


Figure 3

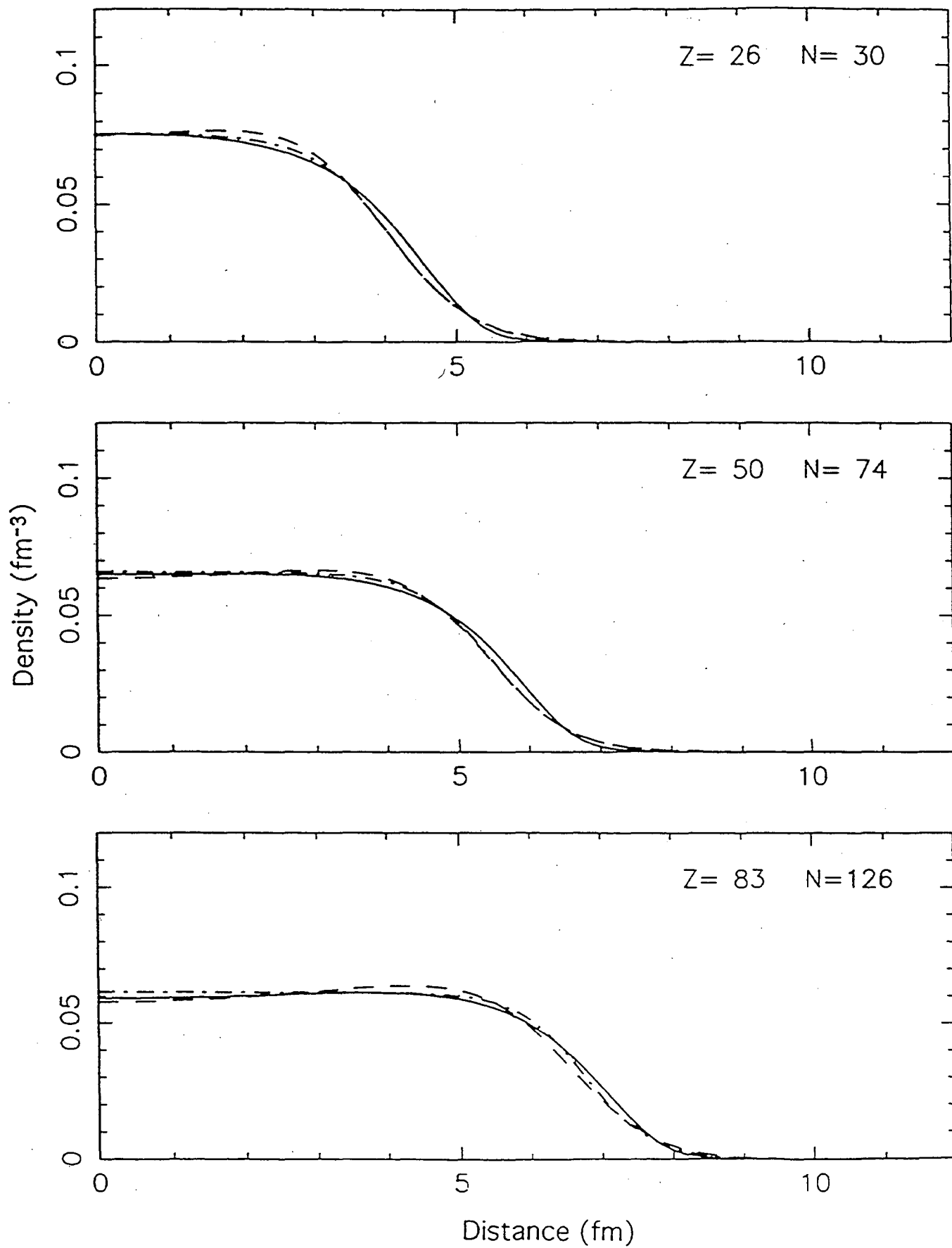


Figure 4

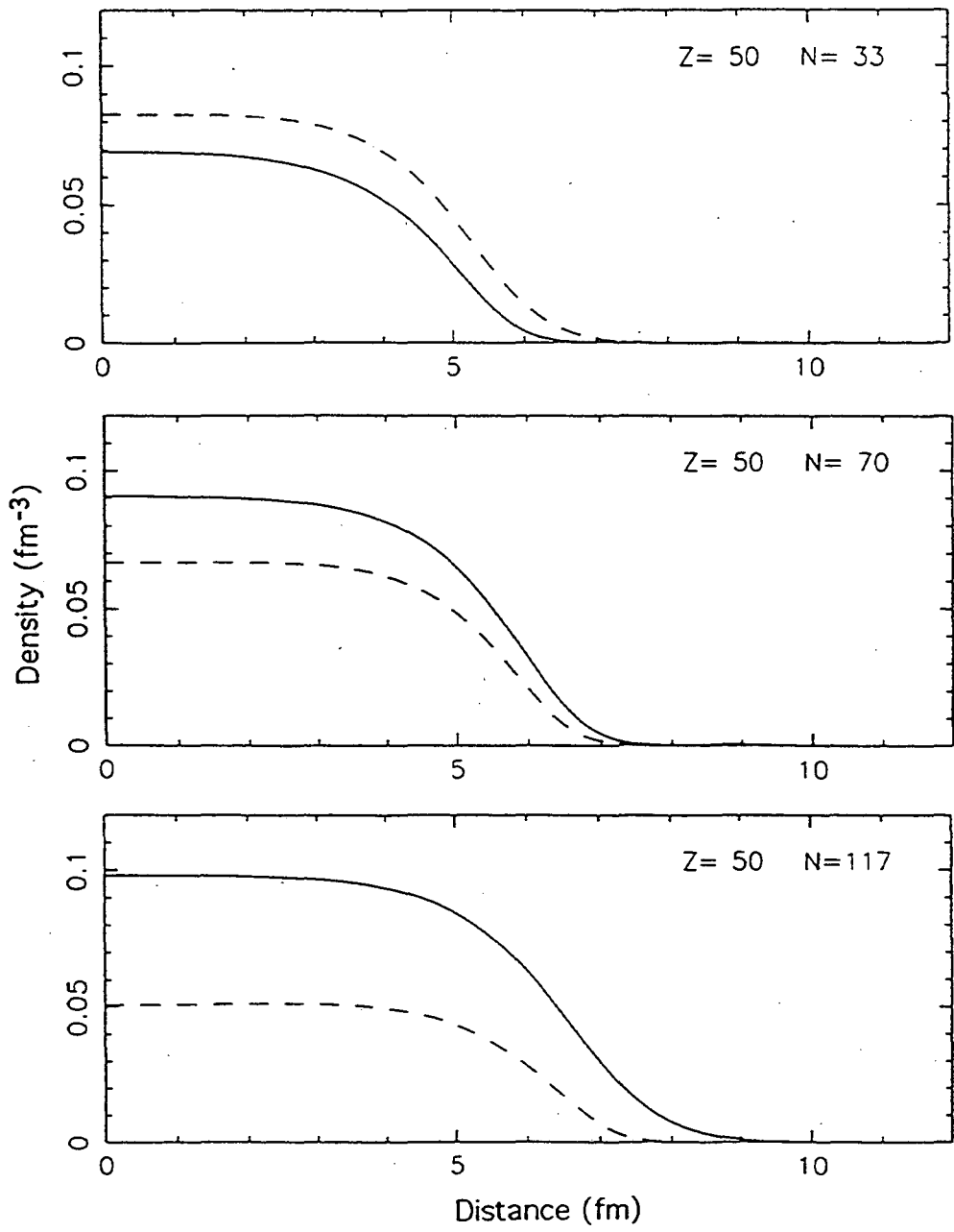


Figure 5

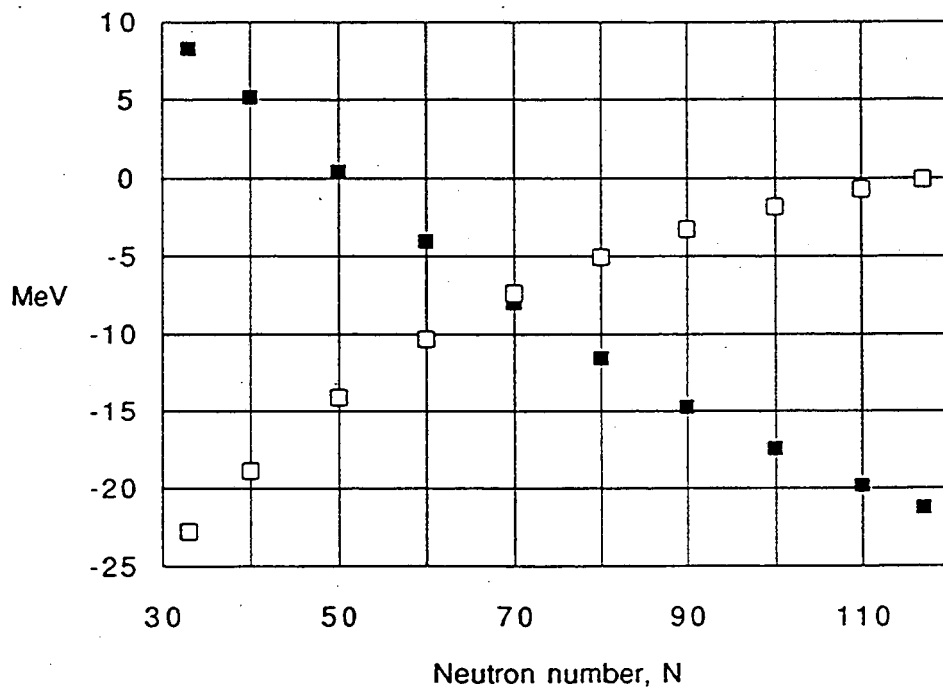


Figure 6

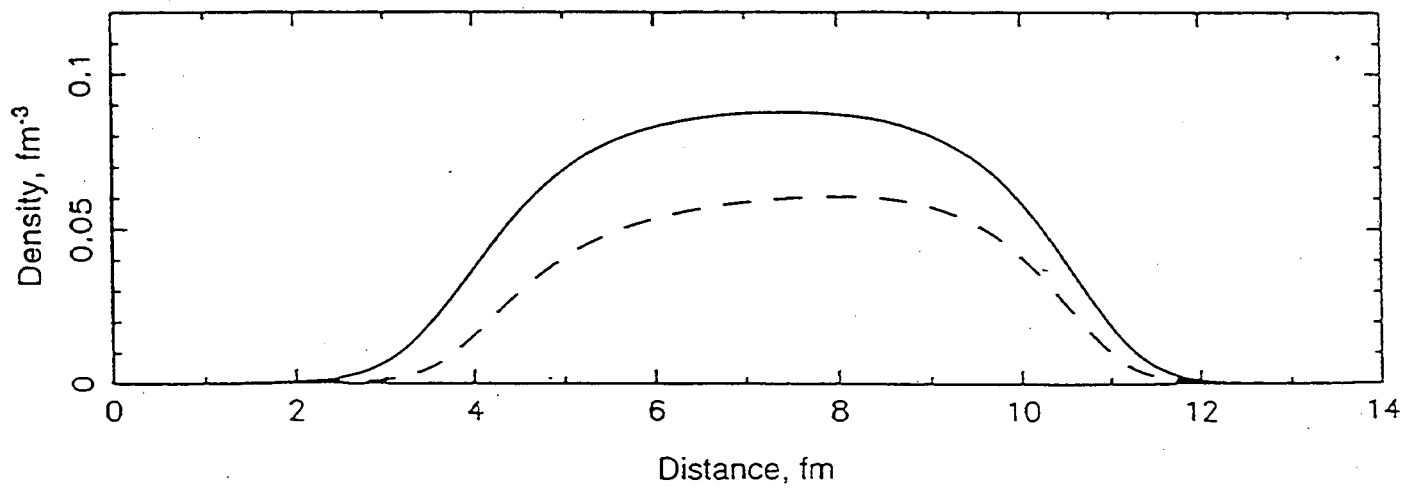
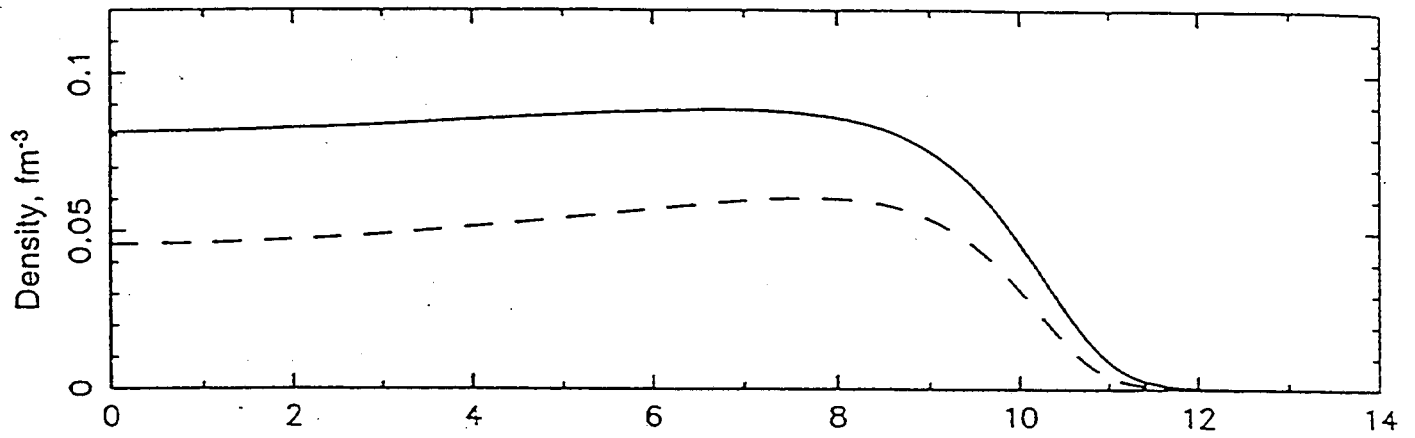


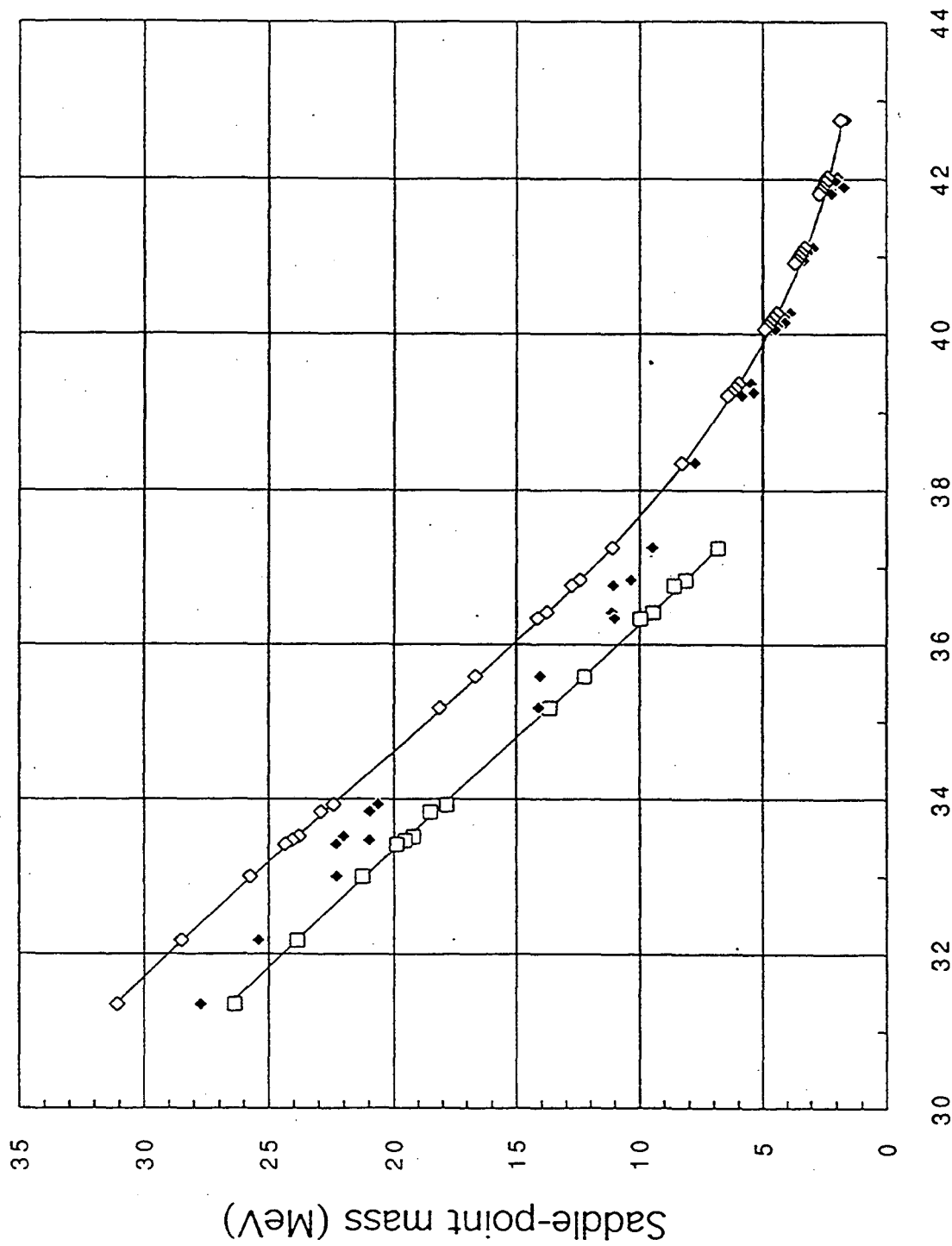
Figure 7

Z \ N-Z	47	48	49	50	51	52	53	54	55	56	57	58	59	60	61	62	63	64	65	66
128											287.93	287.56	288.97	288.81	290.43	290.47	292.29	292.53	294.54	294.98
											0.50	0.94	1.05	1.52	1.52	1.89	(-7.56)	(-7.07)	(-6.83)	(-6.27)
127										279.42	279.14	280.37	280.30	281.73	281.88	283.51	283.85	285.68	286.22	288.25
										-0.75	-0.26	0.06	0.38	0.85	0.99	1.16	1.54	(-7.44)	(-7.01)	(-6.71)
126								268.29	269.41	268.94	270.26	270.00	271.54	271.49	273.22	273.38	275.31	275.67	277.80	278.36
								(-7.21)	(-7.58)	-1.91	-1.57	-1.01	-0.54	-0.14	0.16	0.68	0.76	1.18	1.21	1.52
125							260.23	261.16	260.78	261.91	261.75	263.09	263.14	264.69	264.94	266.69	267.15	269.10	269.76	271.90
							(-6.61)	(-6.97)	(-7.17)	-3.64	-2.96	-2.59	-1.74	-1.15	-0.36	-0.37	0.10	0.24	0.68	0.79
124						250.38	251.40	250.82	252.06	251.69	253.14	252.99	254.64	254.71	256.56	256.84	258.89	259.36	261.62	262.29
						-4.62	-4.94	(-6.10)	(-6.53)	(-6.66)	(-7.03)	-3.68	-3.40	-2.58	-1.82	-1.15	-0.82	-0.22	-0.03	0.46
123					242.59	243.41	242.92	243.96	243.69	244.95	244.90	246.36	246.52	248.19	248.56	250.44	251.01	253.08	253.86	256.13
					-5.59	-5.51	-5.46	-5.63	(-6.15)	(-6.56)	(-6.69)	-5.29	-4.66	-4.39	-3.62	-2.63	-1.98	-1.44	-0.80	-0.54
122				233.00	233.92	233.22	234.36	233.89	235.24	234.99	236.56	236.53	238.30	238.48	240.46	240.85	243.03	243.62	245.99	246.79
				-5.67	-5.92	-5.76	-5.84	-5.73	-5.85	-6.27	-6.56	(-6.21)	-5.77	-5.14	-4.88	-4.16	-3.13	-2.44	-1.73	-0.95
121		226.32	225.48	226.19	225.59	226.53	226.15	227.31	227.16	228.53	228.59	230.18	230.46	232.26	232.74	234.74	235.43	237.63	238.53	240.92
		-5.87	-5.98	-6.30	-6.24	-6.57	-6.50	-6.80	-6.54	-6.75	-6.73	-7.11	-6.75	-6.65	-6.02	-5.76	-5.05	-3.80	-3.39	-2.42
120	217.21	216.16	216.96	216.15	217.18	216.60	217.86	217.50	218.98	218.84	220.53	220.62	222.51	222.81	224.92	225.42	227.73	228.44	230.94	231.86
	-5.53	-5.68	-6.02	-6.12	-6.37	-6.30	-6.81	-6.92	-7.25	-6.77	-7.09	-7.02	-7.36	-6.95	-6.92	-6.31	-6.08	-5.37	-4.39	-3.79
119	208.91	209.51	208.79	209.62	209.13	210.19	209.93	211.20	211.17	212.66	212.85	214.55	214.95	216.87	217.48	219.60	220.42	222.74	223.76	226.28
	-5.45	-5.96	-6.29	-6.71	-6.58	-7.05	-7.15	-7.45	-7.58	-7.89	-7.67	-7.63	-7.75	-8.11	-7.79	-7.73	-7.09	-6.88	-6.18	-5.11
118	200.55	199.61	200.54	199.84	200.99	200.53	201.91	201.67	203.27	203.25	205.06	205.27	207.29	207.71	209.94	210.57	213.00	213.83	216.46	217.50
	-5.52	-5.72	-6.15	-6.25	-6.75	-6.78	-7.20	-7.04	-7.55	-7.52	-7.82	-7.67	-7.89	-7.90	-8.27	-7.83	-7.84	-7.24	-7.05	-6.36
117	192.53	193.25	192.64	193.59	193.22	194.39	194.25	195.65	195.74	197.36	197.66	199.49	200.02	202.06	202.79	205.04	205.98	208.43	209.58	212.22
	-5.52	-6.09	-6.25	-6.72	-6.87	-7.27	-7.33	-7.72	-7.68	-8.03	-8.02	-8.30	-8.21	-8.44	-8.55	-8.96	-8.57	-8.59	-8.02	-7.85
116	184.43	183.61	184.66	184.08	185.35	185.00	186.51	186.39	188.11	188.22	190.16	190.48	192.63	193.17	195.53	196.29	198.85	199.81	202.57	203.73
	-4.77	-5.48	-5.99	-6.18	-6.64	-6.78	-7.21	-7.22	-7.60	-7.50	-7.83	-7.81	-8.07	-8.30	-8.62	-8.70	-8.98	-8.58	-8.63	-8.08
115	176.69	177.53	177.04	178.11	177.86	179.16	179.14	180.66	180.87	182.61	183.04	185.00	185.65	187.82	188.68	191.05	192.12	194.70	195.98	198.76
	-4.96	-5.33	-5.79	-6.30	-6.45	-6.86	-6.95	-7.40	-7.43	-7.84	-7.76	-8.16	-8.17	-8.52	-8.66	-8.98	-9.10	-9.44	-9.09	-9.16
114	168.87	168.16	169.33	168.86	170.27	170.04	171.67	171.67	173.52	173.75	175.82	176.27	178.55	179.22	181.71	182.59	185.28	186.37	189.26	190.55
	-4.84	-5.10	-5.47	-5.28	-6.01	-6.07	-6.47	-6.57	-6.95	-7.00	-7.41	-7.36	-7.74	-7.80	-8.37	-8.61	-8.89	-8.89	-9.12	-8.76
113	161.39	162.36	161.99	163.18	163.05	164.48	164.58	166.23	166.56	168.44	168.99	171.08	171.86	174.16	175.15	177.66	178.85	181.57	182.97	185.88
	-4.96	-5.48	-5.66	-6.03	-5.86	-5.62	-5.11	-5.95	-6.09	-6.54	-6.61	-7.00	-7.04	-7.43	-7.43	-7.76	-7.94	-8.19	-8.37	-8.61
112	153.85	153.26	154.56	154.21	155.74	155.64	157.40	157.52	159.50	159.86	162.06	162.63	165.05	165.84	168.47	169.47	172.30	173.52	176.55	177.97
	-4.91	-5.17	-5.67	-5.91	-6.17	-5.92	-5.77	-5.06	-5.14	-5.17	-5.62	-5.75	-6.19	-6.23	-6.63	-6.64	-6.89	-6.93	-7.29	-7.44
111	146.66	147.74	147.50	148.82	148.81	150.37	150.60	152.38	152.84	154.84	155.52	157.75	158.65	161.09	162.20	164.85	166.18	169.02	170.56	173.61
	-4.96	-5.48	-5.71	-6.20	-6.41	-6.70	-6.38	-6.19	-5.69	-5.36	-5.12	-5.45	-5.43	-5.88	-5.94	-6.34	-6.35	-6.71	-6.49	-6.56
110	139.38	138.92	140.35	140.12	141.79	141.80	143.70	143.95	146.06	146.54	148.88	149.58	152.13	153.06	155.82	156.95	159.92	161.27	164.44	165.99
	-4.93	-5.07	-5.60	-5.85	-6.34	-6.55	-6.79	-6.40	-6.15	-5.61	-5.21	-4.74	-4.91	-4.76	-5.20	-5.22	-5.85	-5.65	-6.01	-5.73
109	132.48	133.69	133.57	135.02	135.14	136.83	137.19	139.10	139.69	141.83	142.64	145.00	146.03	148.61	149.86	152.64	154.10	157.08	158.75	161.94
	-5.04	-5.39	-5.41	-5.93	-6.25	-6.65	-6.92	-7.06	-6.87	-6.38	-5.78	-5.46	-4.81	-4.82	-4.31	-4.77	-4.78	-5.18	-5.20	-5.55
108	125.49	125.14	126.70	126.61	128.40	128.55	130.57	130.95	133.21	133.81	136.29	137.12	139.81	140.87	143.77	145.04	148.15	149.63	152.94	154.62
	-5.07	-4.86	-5.21	-5.27	-5.75	-5.95	-6.38	-6.54	-6.64	-6.23	-5.93	-5.31	-4.90	-4.24	-4.32	-3.68	-4.11	-4.20	-4.64	-4.59
107	118.87	120.21	120.22	121.80	122.05	123.87	124.36	126.41	127.13	129.40	130.35	132.85	134.02	136.72	138.11	141.03	142.63	145.78	147.56	150.89
	-5.19	-5.31	-5.17	-5.37	-5.40	-5.84	-6.00	-6.41	-6.55	-6.61	-6.17	-5.84	-5.26	-4.93	-4.11	-4.23	-4.01	-3.69	-3.72	-4.13
106	112.16	111.94	113.64	113.67	115.60	115.87	118.04	118.55	120.94	121.68	124.30	125.26	128.09	129.28	132.33	133.73	136.98	138.60	142.05	143.88
	-5.07	-4.85	-4.93	-4.63	-4.90	-4.89	-5.30	-5.44	-5.81	-5.91	-5.97	-5.52	-5.18	-4.69	-4.23	-3.52	-3.66	-3.35	-3.11	-3.13

Figure 8

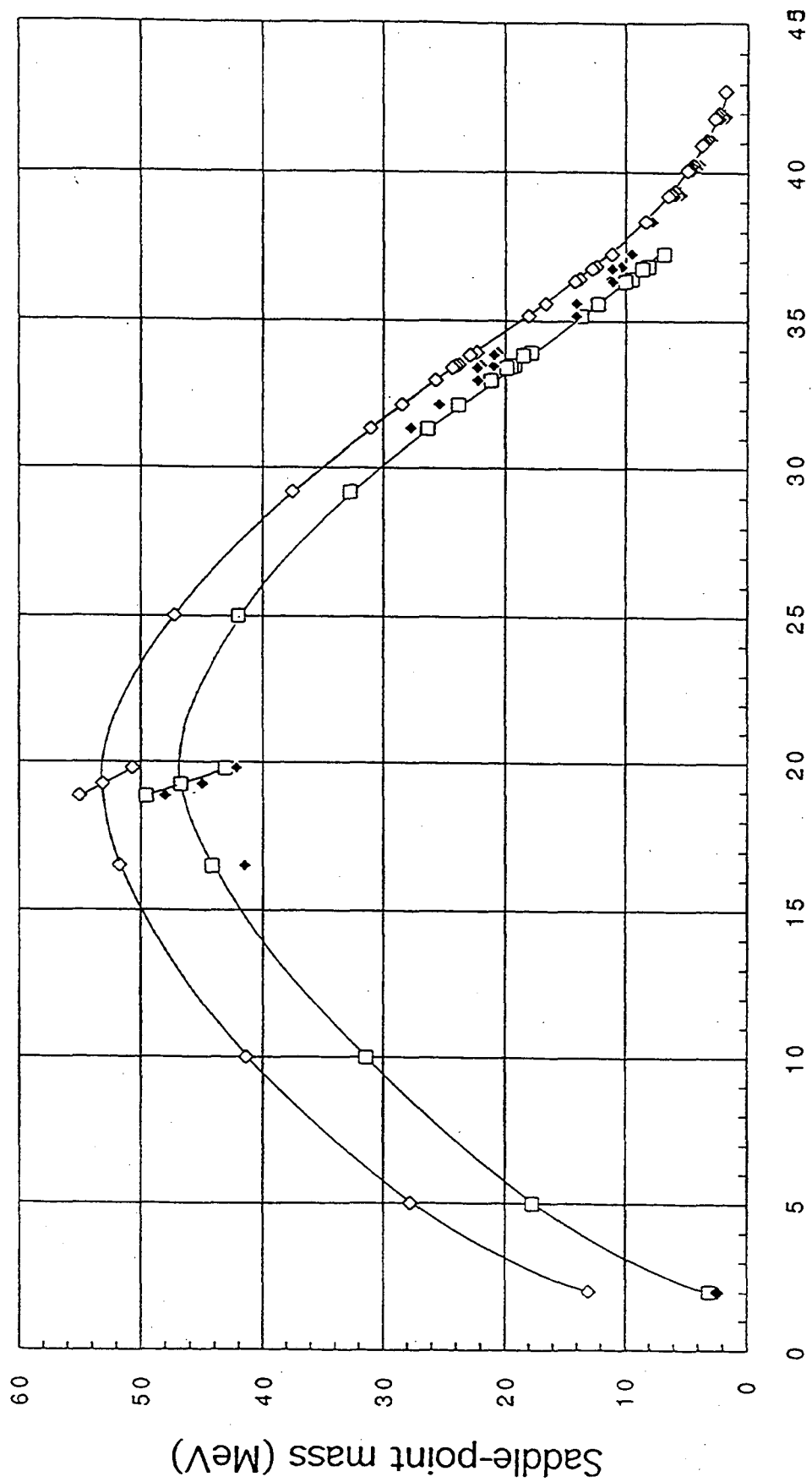
Z	N	A	Fissility	Exp Barr	"Shell"	Congr	TF Lower	Saddle	TF Upper
4	4	8	2.00	0.0	2.28	-10.00	3.11	2.28	13.11
10	10	20	5.00		3.54	-10.00	17.77		27.77
20	20	40	10.00		1.99	-10.00	31.42		41.42
35	40	75	16.49	36.7	4.82	-7.56	44.22	41.52	51.78
42	48	90	19.79	41.8	0.40	-7.56	43.14	42.20	50.70
42	52	94	19.25	45.1	-0.07	-6.40	46.74	45.03	53.14
42	56	98	18.85	45.7	2.34	-5.49	49.54	48.04	55.03
56	76	132	25.02		0.33	-5.29	42.05		47.34
66	94	160	29.19		1.24	-4.80	32.77		37.57
71	102	173	31.35	28.0	-0.28	-4.71	26.37	27.72	31.08
73	106	179	32.18	26.1	-0.69	-4.61	23.88	25.41	28.49
75	110	185	33.00	24.0	-1.70	-4.52	21.24	22.30	25.76
76	110	186	33.52	23.4	-1.38	-4.64	19.20	22.02	23.84
76	111	187	33.47	22.7	-1.70	-4.56	19.54	21.00	24.10
76	112	188	33.42	24.2	-1.89	-4.47	19.89	22.31	24.36
77	112	189	33.93	22.6	-1.98	-4.59	17.83	20.62	22.42
77	114	191	33.84	23.7	-2.75	-4.43	18.50	20.95	22.93
80	118	198	35.17	20.4	-6.32	-4.47	13.66	14.08	18.13
81	120	201	35.59	22.3	-8.26	-4.43	12.23	14.04	16.66
83	124	207	36.42	21.9	-10.78	-4.35	9.45	11.12	13.80
83	126	209	36.35	23.3	-12.28	-4.21	9.97	11.02	14.18
84	126	210	36.84	20.95	-10.62	-4.32	8.12	10.33	12.44
84	128	212	36.77	19.5	-8.45	-4.18	8.60	11.05	12.78
85	128	213	37.26	17.0	-7.51	-4.28	6.84	9.49	11.12
88	140	228	38.35	8.1	-0.34	-3.84		7.76	8.32
90	138	228	39.36	6.5	-1.00	-4.13		5.50	5.99
90	140	230	39.30	7.0	-0.94	-4.01		6.06	6.16
90	142	232	39.25	6.3	-0.92	-3.90		5.38	6.31
90	144	234	39.21	6.65	-0.79	-3.79		5.86	6.45
92	140	232	40.28	5.4	-1.53	-4.19		3.87	4.45
92	142	234	40.21	5.8	-1.72	-4.08		4.08	4.60
92	144	236	40.15	5.75	-1.65	-3.96		4.10	4.73
92	146	238	40.11	5.9	-1.50	-3.86		4.40	4.84
92	148	240	40.07	5.8	-1.30	-3.75		4.50	4.94
94	144	238	41.12	5.3	-2.39	-4.14		2.91	3.31
94	146	240	41.06	5.5	-2.36	-4.03		3.14	3.43
94	148	242	41.00	5.5	-2.18	-3.92		3.32	3.53
94	150	244	40.96	5.3	-1.97	-3.81		3.33	3.62
94	152	246	40.92	5.3	-1.72	-3.71		3.58	3.71
96	146	242	42.03	5.0	-3.07	-4.20		1.93	2.36
96	148	244	41.96	5.0	-3.05	-4.09		1.95	2.46
96	150	246	41.91	4.7	-2.99	-3.98		1.71	2.55
96	152	248	41.86	5.0	-2.79	-3.87		2.21	2.62
96	154	250	41.82	4.4	-2.23	-3.77		2.17	2.69
98	154	252	42.76	4.8	-3.20	-3.93		1.60	1.84

Figure 9



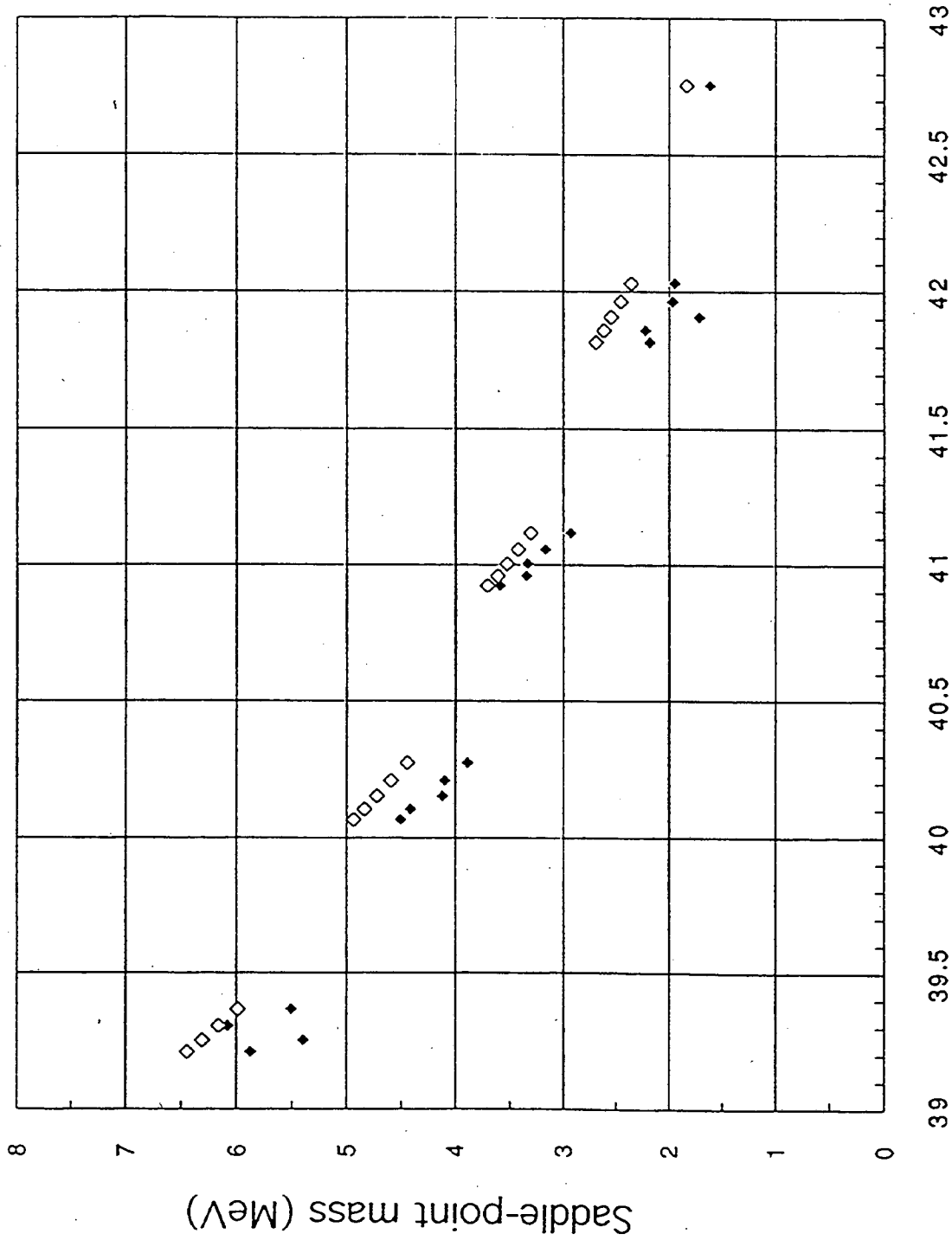
Fissility

Figure 10



Fissility

Figure 11



Fissility

Figure 12

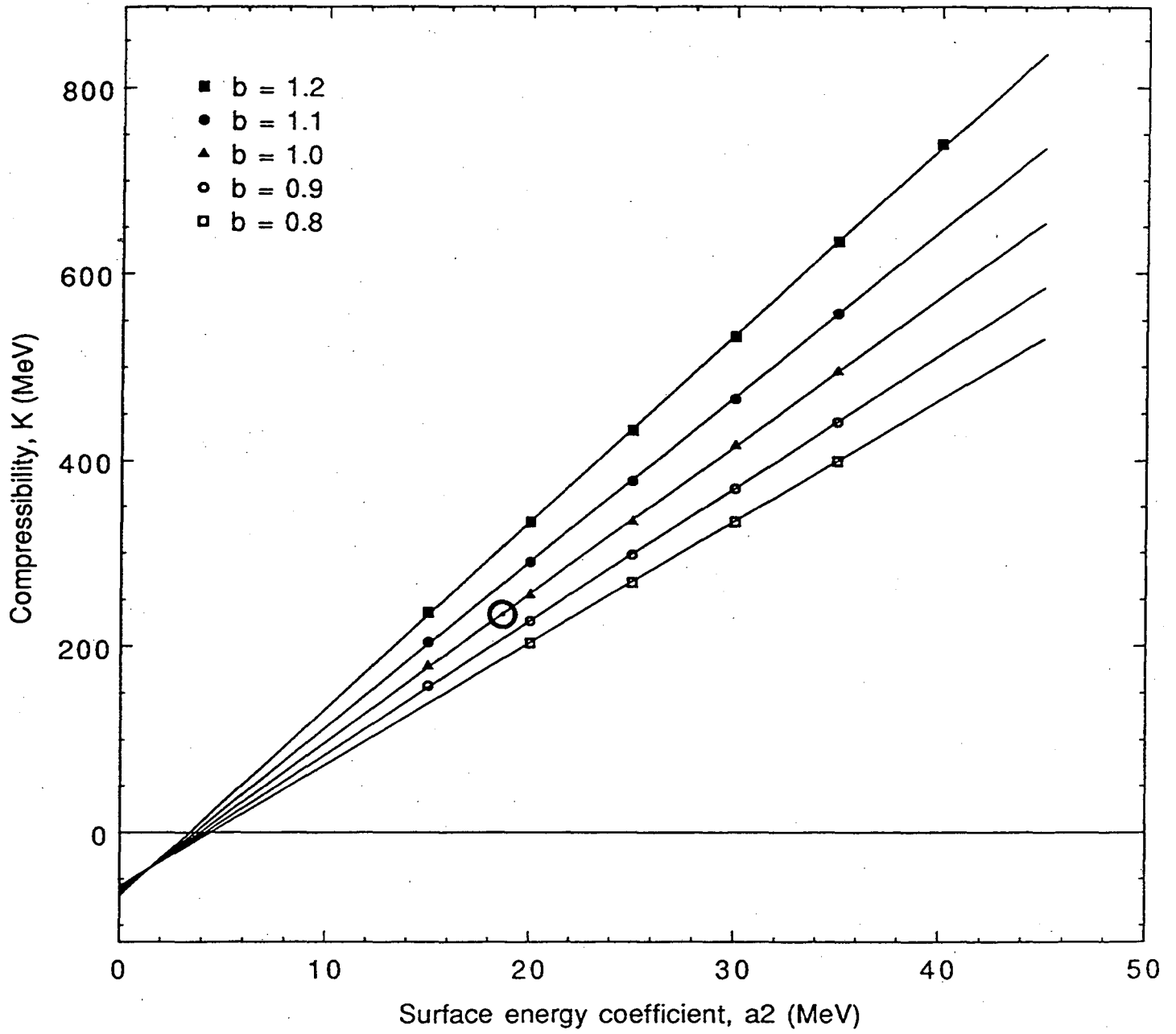
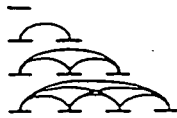


Figure 13

No. of particles
in identical orbits No. of pairs

1	0
2	1
3	3
4	6



	N	Z	Number of identical pairs
even-even			$\frac{3}{2}A - N - Z $
odd-even			$\frac{3}{2}A - N - Z - \frac{1}{2}$
even-odd			
odd-odd			$\frac{3}{2}A - N - Z - 1$
odd-odd N = Z			$\frac{3}{2}A - 2$

Figure 14

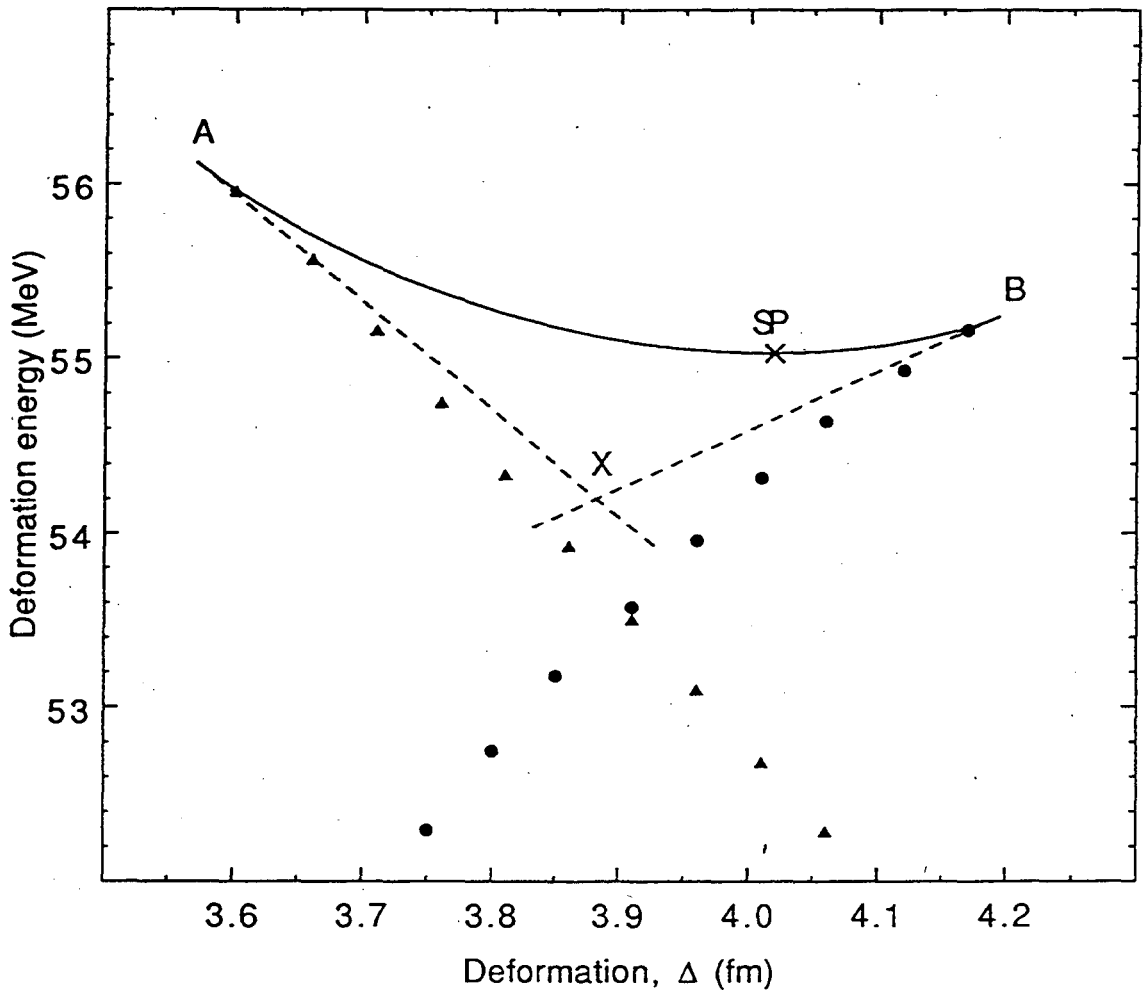


Figure 15

LAWRENCE BERKELEY LABORATORY
UNIVERSITY OF CALIFORNIA
TECHNICAL AND ELECTRONIC
INFORMATION DEPARTMENT
BERKELEY, CALIFORNIA 94720